PHYSICAL REVIEW C VOLUME 15, NUMBER 5 MAY 1977

Even-parity states of ^{95}Tc

L. D. Skouras
Tandem Accelerator Laboratory, N. R. C. Demokritos, Aghia Paraskevi Attikis, Greece

C. Dedes
Department of Physics, University of Ioannina, Ioannina, Greece

(Received 21 July 1976; revised manuscript received 13 December 1976)

An attempt is made to explain the observed even-parity spectrum and transition rates of ^{95}Tc. The shell-model approach is followed and the three valence protons are restricted to the $0g_{9/2}$ orbital. On the other hand, full configuration mixing has been assumed for the two valence neutrons which are allowed to take all possible values in the $1d_{5/2}$, $2s_{1/2}$, $1d_{3/2}$, and $0g_{7/2}$ orbitals. Experimental single particle energies are used in the calculation while the two-body matrix elements are derived from the Sussex and Yale interactions by means of second order perturbation theory. Thus, using only one free parameter, namely the effective charge, we have reproduced to a good approximation the excitation energies and transition rates of about 35 observed levels. In addition, the calculation predicts a number of levels that, quite possibly, have not yet been experimentally observed.

[NUCLEAR STRUCTURE ^{95}Tc, calculated positive-parity levels, $B(E2)$, $B(M1)$, $T_{1/2}$, branching ratios.]

I. INTRODUCTION

Recently several experimental and theoretical investigations have been devoted to the study of the odd-mass[93,95,97,99] Tc isotopes. According to the shell model these isotopes can be described in terms of three $0g_{9/2}$ protons coupled to an even number of neutrons beyond the $N=50$ neutron "core."

In most of the theoretical work reported on the study of the Tc isotopes the neutrons have been treated as a vibrating core.[1-4] Comparison of the low-lying positive-parity levels of ^{95,97,99}Tc with the extended quasiparticle-phonon model of Goswami and Nalcioglu[1] and with the core-coupling calculations of Goswami, McDaniels, and Nalcioglu,[2] has demonstrated[7,8] that these theories are not in satisfactory agreement with experiment. In a different approach Xenoulis[3] considers the coupling of a $0g_{9/2}$ quasiparticle proton to a slightly deformed core. In this way he interprets the five lowest positive-parity levels of ^{95}Tc as band-heads on which rotational states are built. However, this theory is still incomplete since no projection of good angular momentum states was performed on these intrinsic states. The most detailed theoretical study on ^{95}Tc has been performed by Bargholtz and Beshai,[4] who considered the coupling of the $(0g_{9/2})^3$ proton cluster to the vibrating core. Considering up to four-phonon excitations, they were able to account for many of the observed energy levels and transition rates of this nucleus.

It should be pointed out that the above phenomenological calculations suffer from two main drawbacks: (a) they consider the interaction of the neutrons beyond $N=50$, only in a very average way, and (b) they use a varying number of parameters adjusted to produce best agreement with experiment.

A more fundamental approach to the study of the Tc isotopes ought to employ the shell-model scheme. This is because in that approach the interactions of the neutrons beyond the $N=50$ "core" as well as the proton-neutron interaction can be calculated explicitly. Moreover, in a "realistic" shell-model approach the matrix elements of the "effective" interaction are evaluated from the "bare" G matrix, thus reducing considerably the number of free parameters.

Shell-model calculations on the $A \geq 95$ Tc isotopes have been reported so far by Vervier,[5] and Bhatt and Ball.[6] However, in these calculations only the simple $(0g_{9/2}p)^3(1d_{5/2}n)^k$ basis was employed, while the matrix elements of the effective interaction were treated as parameters deduced from the experimental spectra of ^{92}Mo, ^{92}Zr, and ^{92}Nb. At the time when these shell-model calculations were reported, detailed comparison between theory and experiment was not possible due to the lack of enough experimental data. Due, however to the neglect of configuration mixing, one could not expect this simple model to reproduce anything but the gross features of the examined nuclei.

Recently detailed experimental information[9-12] has become available about the energy spectrum and the transition rates of ^{95}Tc. In particular, Sarantites and Xenoulis[9] studying the ^{95}Mo$(p,n\gamma)^{95}$Tc reaction have established the position, spin,

and decay properties of many levels with $J^\pi \leq \frac{13}{2}+$ up to 2324 keV. On the other hand, the study of a number of high-spin levels ($J \leq \frac{33}{2}$) has been accomplished with the use of the ^{93}Nb$(\alpha, 2n\gamma)^{95}$Tc reaction.[10-12] The energy spectrum of the known positive-parity states of ^{95}Tc is shown in Figs. 2, 3, and 4. The presence of levels with $J^\pi > \frac{29}{2}+$ clearly indicates that configurations with neutrons in the $0g_{7/2}$ orbital play an important role in the even-parity spectrum of ^{95}Tc.

In the present work an attempt is made to explain the energy spectrum and the decay properties of the positive-parity states of ^{95}Tc. Our model differs from the previously mentioned shell-model calculations in the respect that full configuration mixing between neutrons is allowed, while the effective interaction is evaluated in a realistic way. There are two reasons for selecting ^{95}Tc among the other Tc isotopes for such a realistic calculation. The first is that the number of valence particles is not too large and therefore a detailed treatment of configuration mixing can be made. The second reason is that experimental information on ^{95}Tc is by far the most complete in comparison with the other Tc isotopes, thus permitting a rather detailed comparison between theory and experiment.

Details of the model are discussed in Sec. II, while the comparison between theory and experiment is given in Sec. III.

II. THE MODEL

A. Description of the model space

As indicated in the introduction, the basis vectors considered in this work for the description of the positive-parity states of ^{95}Tc have the general form

$$|^{95}\mathrm{Tc}; JM\rangle = |(0g_{9/2}p)^3 J_p, (1d_{5/2}, 2s_{1/2}, 1d_{3/2}, 0g_{7/2}n)^2 J_n; JM\rangle \ . \tag{1}$$

As may be seen from (1), the three valence protons are restricted to the $0g_{9/2}$ orbital. This is a reasonable approximation as far as proton excitation to the other orbitals of the *sdg* shell are concerned. These orbitals are expected to lie about $\hbar\omega \sim 9$ MeV higher than the $0g_{9/2}$ orbital, and this large energy gap secures the validity of this approximation. A more serious approximation, followed in the present work, is to neglect all those configurations that involve two-proton excitations from the $0f$-$1p$ shell to the $0g_{9/2}$ orbital. The $0f$-$1p$ shell orbitals lie quite close to the $0g_{9/2}$ and therefore, on energy grounds, one would expect that these configurations should be important. However, recent realistic shell-model calculations on ^{90}Zr, ^{92}Mo, ^{93}Tc, and ^{94}Ru reported by Dedes and Irvine[13,14] show that, while proton configurations of the type $(0g_{9/2})^n (0f\text{-}1p)^{-2}$ play a vital role in ^{90}Zr, their effects are much smaller for the other three nuclei. For this reason, in the present work, configurations of the type $(0g_{9/2})^5(0f\text{-}1p)^{-2}$ were neglected from the model space. Nevertheless, the effects of the $0f$-$1p$ shell have been considered in the evaluation of the effective interaction (Sec. II B).

In Fig. 1 the energy spectrum of the $(0g_{9/2})^3$ proton configurations is compared with the observed levels of ^{93}Tc.[15] Figure 1 shows that the simple $(0g_{9/2})^3$ configurations account satisfactorily for the energies of all the observed levels of ^{93}Tc up to 2.5 MeV. Direct evidence for the importance of other configurations appears by the presence of a $\frac{25}{2}+$ level in the spectrum of ^{93}Tc. However, this level is quite high in energy (4257 keV) and therefore its configuration is not expected to play a vital role in the low-lying states of ^{95}Tc.

The usual shell-model Hamiltonian is adopted:

$$H = \sum_i \epsilon_i a_i^\dagger a_i + \frac{1}{2} \sum_{klmn} \langle kl \,|V|\, mn\rangle a_k^\dagger a_l^\dagger a_n a_m \ . \tag{2}$$

The calculation of the matrix elements of the effective interaction is discussed in Sec. II B. The experimental values are used for the single-particle energies of the neutron orbitals. These are given by

$$\epsilon_{d_{5/2}} = 0, \quad \epsilon_{s_{1/2}} = 1.0 \text{ MeV}, \quad \epsilon_{d_{3/2}} = 2.50 \text{ MeV}, \quad \epsilon_{g_{7/2}} = 3.0 \text{ MeV}, \tag{3}$$

and are quoted by Vergados and Kuo[16] in their calculation of $E1$ transitions on ^{88}Sr and ^{90}Zr.

It is clear from (3) that the $2s_{1/2}$, $1d_{3/2}$, and $0g_{7/2}$ neutron orbitals are not very much separated from the $1d_{5/2}$. Therefore, the approximation made in earlier calculations[5,6] of considering only the $(1d_{5/2})^2$ neutron configurations has not been followed here. Thus full configuration mixing has been assumed by allowing the two neutrons to take all possible values in the $1d_{5/2}$, $2s_{1/2}$, $1d_{3/2}$, and $0g_{7/2}$ orbitals.

Harmonic oscillator wave functions have been used throughout the calculation and the oscillator parameter b has been given the appropriate value for this mass region of 2.1 fm.

B. Calculation of the effective interaction

As mentioned earlier, in the present work we follow the realistic calculation approach, introduced by Kuo and Brown.[17,18] With the basis defined by (1), the two-body part of the shell-model Hamiltonian is conveniently represented in the following schematic way:

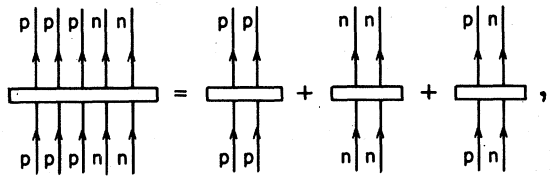

(4)

where $p = 0g_{9/2}$ and $n = (1d,\ 2s,\ 0g_{7/2})$ denote proton and neutron states, respectively. The boxes in (4) imply the corresponding effective interactions, while the free fermion lines which accompany each effective interaction are conveniently omitted. The first approximation implied by (4) is the neglect of the effective three-body interactions. Their effects are currently studied in a much simpler case.[19] However, these three-body forces are not expected to have large effects on the energy spectra.

For the evaluation of the two-body effective interactions we made the three simplifying assumptions, i.e., (a) that the orbitals of each major shell are degenerate, (b) that the energy separation between two successive shells is $\hbar\omega$, and finally (c) that diagrams with energy denominators exceeding $2\hbar\omega$ should be neglected. For comparison, two forms of realistic interactions, namely the Yale[20] and the Sussex[21] interactions, have been employed in the present work.

The calculation of effective interaction between protons in the $0g_{9/2}$ orbital has been reported previously[13] and therefore it will not be mentioned here. In the calculation of the n-n effective interaction, the following diagrams are considered:

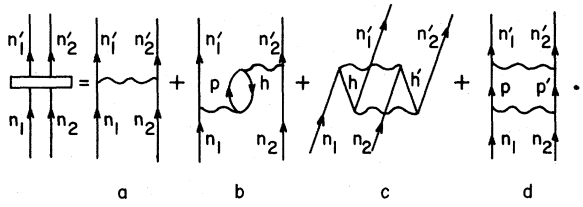

(5)

Only the direct Goldstone graphs are shown in (5). To be consistent with earlier calculations,[13,14] the ladder diagram is only evaluated for the Sussex interaction, while it is omitted for the Yale interaction, which thus is interpreted as a G matrix. Parity conservation requires that all intermediate states would be of even parity. Neutron "particle" states correspond to orbitals beyond the $0g_{9/2}$, while neutron "hole" states correspond to orbitals inside the $N = 50$ core.

The conservation of the number of particles requires that all intermediate single-particle states shown in (5c) and (5d) are neutron states. However, this restriction does not hold for the "core polarization" diagram (5b), where the p-h bubble can involve proton states as well. In the latter case the proton particle states are those outside the $Z = 40$ proton core and the corresponding proton hole states are clearly those inside the $Z = 40$ core.

The same diagrams (5) are also used in the evaluation of the p-n effective interaction. Clearly the core polarization diagram (5b) corresponds to the four exchange terms:

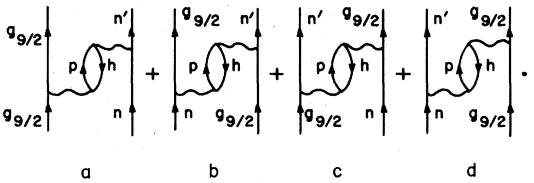

(6)

In diagrams (6a) and (6d) the p-h bubble is either a proton or a neutron bubble. However, diagrams (6b) and (6c) represent physically different pro-

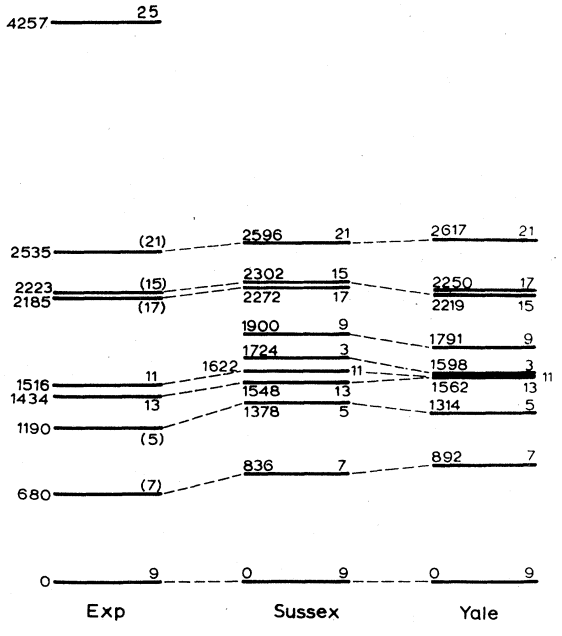

FIG. 1. Comparison of experimental (Ref. 15) and theoretical spectra of ^{93}Tc. The two theoretical spectra have been calculated using the $(0g_{9/2})^3$ configurations. The number on the right of each level corresponds to $2J$ while the number on the left gives the excitation energy in keV.

cesses. Diagram (6b), for example, could be interpreted in terms of the exchange of a proton with a neutron inside the core leaving a proton hole, while due to the exclusion principle the extra neutron is raised outside the core. Evidently in (6b) the particle state in the bubble is a neutron state while the hole state is a proton hole. In an analogous manner the bubble in (6c) consists of a proton particle and a neutron hole.

As expected, it is found that the core polarization terms (5b) and (6) are the major correcting contributions in the construction of the effective interactions. In particular, for the interaction between neutrons the main contribution comes from a proton p-h bubble. This is understandable because in this case both the $T=0$ and $T=1$ terms are contributing to the matrix elements.

The matrix elements of the n-n and p-n effective interactions calculated in this work are listed in Tables I and II, respectively. The matrix elements deduced by Bhatt and Ball[6] are compared with those calculated in this work in Tables III(a) and III(b). To make such a comparison complete we also give in Table III (c) the p-p matrix elements calculated earlier.[13] It may be seen from Table III that our matrix elements are not very different from those obtained by Bhatt and Ball.[6] The existing differences should be attributed not only to the different model spaces adopted, but also to the different approaches followed in the two calculations.

III. RESULTS OF THE CALCULATION

In this section the results obtained with the present model, as introduced in Sec. II, are compared with experiment. It is useful to classify the experimental information on ^{95}Tc into three parts. The first part contains the information about the even-parity states of ^{95}Tc up to 1433 keV. The spin, parity, and decay scheme of these levels are known rather unambiguously[9,10,12,22-24] and thus comparison between theory and experiment on this part of the spectrum is practicable. This comparison is made in Sec. III A.

TABLE I. The matrix elements $\langle n_1 n_2 J \mid V_{\text{eff}} \mid n_1 n_2 J\rangle$ of the neutron-neutron effective interaction. The numbers 1, 2, 3, and 4 correspond to the $0g_{7/2}$, $1d_{5/2}$, $1d_{3/2}$, and $2s_{1/2}$ neutron orbitals, respectively. The matrix elements are measured in MeV.

$n_1n_2n_1'n_2'$	J	Sussex	Yale	$n_1n_2n_1'n_2'$	J	Sussex	Yale	$n_1n_2n_1'n_2'$	J	Sussex	Yale
1111	0	−1.1614	−0.9162	1222	2	0.0615	0.0810	2222	0	−0.7936	−0.6371
	2	−0.3620	−0.2730		4	0.0470	0.0501		2	−0.3379	−0.2793
	4	0.0683	0.1591	1223	1	0.0047	0.0087		4	−0.0912	−0.0228
	6	0.2201	0.3339		2	0.1237	0.1075	2223	2	−0.0840	−0.0897
1112	2	−0.0261	−0.0169		3	−0.0344	−0.0188		4	−0.3660	−0.3668
	4	0.0622	0.0687		4	0.1543	0.1460	2224	2	−0.3500	−0.3143
	6	0.0797	0.0452	1224	2	0.1138	0.1020	2233	0	−1.1811	−1.1034
1113	2	−0.2510	−0.2062		3	−0.0349	−0.0460		2	−0.2421	−0.2628
	4	−0.1403	−0.1069	1233	2	0.0151	0.0051	2234	2	0.2548	0.2532
1114	4	0.0557	0.0401	1234	1	−0.0608	−0.0767	2244	0	−0.4567	−0.3686
1122	0	−0.6342	−0.5803		2	−0.0584	−0.0639	2323	1	−0.0215	−0.0227
	2	−0.1246	−0.1366	1313	2	−0.4250	−0.3376		2	−0.1200	−0.0545
	4	−0.0772	−0.0868		3	0.0504	0.0841		3	−0.0520	−0.0412
1123	2	−0.1267	−0.1190		4	0.0757	0.1575		4	−0.5769	−0.4784
	4	−0.1359	−0.1205		5	0.0513	0.1198	2324	2	−0.1137	−0.1005
1124	2	−0.1727	−0.1616	1314	3	−0.1181	−0.0924		3	−0.0826	−0.0702
1133	0	−0.4189	−0.3266		4	0.1768	0.1445	2333	2	−0.2844	−0.2903
	2	−0.1201	−0.0972	1322	2	−0.1238	−0.1129	2334	1	−0.0027	0.0028
1134	2	0.0743	0.0514		4	−0.0058	0.0224		2	0.3063	0.2882
1144	0	−0.2500	−0.1845	1323	2	−0.2162	−0.2025	2424	2	−0.5196	−0.4520
1212	1	−0.2538	−0.2267		3	−0.0059	−0.0089		3	−0.0682	−0.0040
	2	−0.0591	−0.0012		4	−0.1394	−0.1146	2433	2	−0.2659	−0.2413
	3	−0.0555	−0.0466	1324	2	−0.2110	−0.1858	2434	2	0.5355	0.5297
	4	0.0471	0.0998		3	−0.0564	−0.0775	3333	0	−0.3526	−0.2228
	5	0.0272	0.0272	1333	2	−0.2001	−0.1738		2	−0.0238	0.0434
	6	−0.3732	−0.2394	1334	2	0.2130	0.1865	3334	2	0.1338	0.1026
1213	2	0.2727	0.2713	1414	3	0.0355	0.0759	3344	0	−0.3890	−0.2946
	3	0.0960	0.0961		4	−0.1262	−0.0606	3434	1	0.0341	0.0591
	4	0.1576	0.1611	1422	4	0.0908	0.0782		2	−0.2511	−0.1647
	5	−0.0606	−0.0530	1423	3	−0.0216	−0.0229	4444	0	−0.8392	−0.7245
1214	3	−0.1348	−0.1230		4	0.1637	0.1152				
	4	−0.2783	−0.2477	1424	3	0.0339	0.0435				

TABLE II. The matrix elements $\langle p_1 n_1 J | V_{\text{eff}} | p_2 n_2 J \rangle$ of the proton-neutron effective interaction. The number 5 refers to the $0g_{9/2}$ proton orbital. The numbers 1, 2, 3, and 4 correspond to the $0g_{7/2}$, $1d_{5/2}$, $1d_{3/2}$, and $2s_{1/2}$ neutron orbitals, respectively. The matrix elements are measured in MeV.

$p_1 n_1 p_2 n_2$	J	Sussex	Yale	$p_1 n_1 p_2 n_2$	J	Sussex	Yale	$p_1 n_1 p_2 n_2$	J	Sussex	Yale
5151	1	−1.8523	−2.2794	5153	3	−0.2142	−0.2566	5253	3	0.4687	0.4654
	2	−1.3419	−1.5222		4	−0.3109	−0.3254		4	−0.0591	−0.0820
	3	−0.5999	−0.6207		5	−0.1383	−0.1406		5	0.2115	0.2365
	4	−0.5985	−0.7195		6	−0.3330	−0.2908		6	−0.1652	−0.1431
	5	−0.2288	−0.2569	5154	4	−0.1355	−0.0968	5254	4	−0.2489	−0.2026
	6	−0.6124	−0.7269		5	0.0387	0.0624		5	−0.3852	−0.3829
	7	−0.0478	−0.0188	5252	2	−0.8138	−0.6607	5353	3	−0.7921	−0.8431
	8	−1.1979	−1.1523		3	−0.3333	−0.2925		4	−0.3395	−0.3078
5152	2	−0.4511	−0.3922		4	−0.1658	−0.1067		5	−0.1195	−0.1488
	3	0.0077	0.0486		5	−0.2111	−0.2069		6	−0.5539	−0.4432
	4	−0.0980	−0.0700		6	−0.0842	−0.0274	5354	4	−0.2994	−0.2483
	5	0.0891	0.1265		7	−0.7193	−0.6978		5	0.2681	0.3061
	6	−0.0511	−0.0165					5454	4	−0.2478	−0.1834
	7	0.1466	0.1931						5	−0.4075	−0.3989

Many levels have been observed[9] between 1433 and 2324 keV. However, definite J^π values have not yet been assigned to most of these levels, while their decay scheme is only partially known. The calculation predicts a large number of levels in this energy region. Based on the available experimental data one can tentatively identify some of the theoretical states with observed levels. This identification is discussed in Sec. III B.

Finally, the study of the ^{93}Nb$(\alpha, 2n\gamma)^{95}$Tc reaction[10–12] has established a number of high-spin levels between 1515 and 5604 keV. The predictions of the model on high-spin levels are compared with experiment in Secs. III C and III D.

TABLE III. The matrix elements $\langle 1d_{5/2})^2 J | V_{\text{eff}} | \times (1d_{5/2}{}^2 J \rangle$, $\langle 0g_{9/2} 1d_{5/2}, J | V_{\text{eff}} | 0g_{9/2} 1d_{5/2}, J \rangle$, and $\langle (0g_{9/2})^2 J | V_{\text{eff}} | (0g_{9/2})^2 J \rangle$ of the (a) neutron-neutron, (b) proton-neutron, and (c) proton-proton effective interactions, respectively. Fitted values for the neutron-neutron and the proton-neutron interactions are taken from Ref. 6. Sussex and Yale values for the proton-proton interaction are taken from Ref. 13, and fitted values from Ref. 16.

J	Sussex	Yale	Fitted
	(a) $\langle (1d_{5/2})^2 J | V_{\text{eff}} | (1d_{5/2})^2 J \rangle$		
0	−0.7936	−0.6371	−1.31
2	−0.3379	−0.2793	−0.39
4	−0.0912	−0.0228	0.18
	(b) $\langle 0g_{9/2} 1d_{5/2}, J | V_{\text{eff}} | 0g_{9/2} 1a_{5/2}, J \rangle$		
2	−0.8138	−0.6607	−0.57
3	−0.3333	−0.2925	−0.42
4	−0.1658	−0.1067	−0.23
5	−0.2111	−0.2069	−0.35
6	−0.0842	−0.0274	−0.21
7	−0.7193	−0.6978	−0.71
	(c) $\langle (0g_{9/2})^2 J | V_{\text{eff}} | (0g_{9/2})^2 J \rangle$		
0	−2.4635	−2.3106	−2.25
2	−0.8267	−0.6659	−0.71
4	−0.1582	−0.0718	0.08
6	0.1208	0.2073	0.41
8	0.2351	0.3859	0.55

A. Even parity-levels of ^{95}Tc up to 1433 keV

The low-lying even-parity spectra calculated with the Sussex and Yale effective interactions are shown in Fig. 2 together with the experimental spectrum.[9,10,12,22–24] As Fig. 2 shows, all observed even-parity states up to 1433 keV are ac-

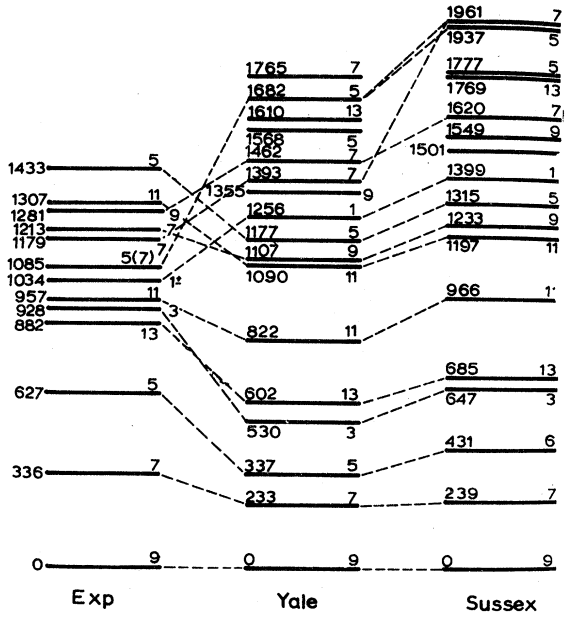

FIG. 2. The experimental (Refs. 9, 10–12, 22–24) and calculated even parity spectra of ^{95}Tc up to 1433 keV. The number on the right of each level corresponds to $2J$.

TABLE IV. Experimental and calculated transition rates of the even-parity states of ^{95}Tc up to 1433 keV.

Initial state		Final state		Experiment[a]			
E (keV)	J^π	E (keV)	J^π	$M1$ (W.u.)	$E2$ (W.u.)	Branch (%)	T_m (fs)
336	$\frac{7}{2}^+$	0	$\frac{9}{2}^+$			100	
627	$\frac{5}{2}^+$	0	$\frac{9}{2}^+$			82.2	
		336	$\frac{7}{2}^+$			17.8	
882	$\frac{13}{2}^+$	0	$\frac{9}{2}^+$		35^{+24}_{-16}	100	1700^{+1300}_{-700}
928	$\frac{3}{2}^+$	336	$\frac{7}{2}^+$		≤ 120	34.1	≥ 1700
		627	$\frac{5}{2}^+$	≤ 0.61	≤ 300	65.9	
957	$\frac{11}{2}^+$	0	$\frac{9}{2}^+$	3.3×10^{-3}	17 ± 5	100	1900^{+1200}_{-700}
		336	$\frac{7}{2}^+$			≤ 2	
1034	$\frac{1}{2}^+$	627	$\frac{5}{2}^+$				
		928	$\frac{3}{2}^+$				
1085	$\frac{5}{2}^+$	0	$\frac{9}{2}^+$			1.8	
		336	$\frac{7}{2}^+$			95	≥ 500
		627	$\frac{5}{2}^+$			3.2	
		928	$\frac{3}{2}^+$			<1	
1179	$\frac{7}{2}^+$	0	$\frac{9}{2}^+$	$(16\pm5)\times10^{-3}$	$1.9^{+1.5}_{-0.8}$	51.2	
		336	$\frac{7}{2}^+$	$(21\pm7)\times10^{-3}$	≤ 4.5	21.1	≥ 500
		627	$\frac{5}{2}^+$	$(94\pm31)\times10^{-3}$	15^{+16}_{-12}	27.7	
		1085	$\frac{5}{2}^+$				
1213	$\frac{9}{2}^+$	0	$\frac{9}{2}^+$			9.3	
		336	$\frac{7}{2}^+$			90.7	
		957	$\frac{11}{2}^+$				
1281	$\frac{7}{2}^+$	0	$\frac{9}{2}^+$	$(70\pm35)\times10^{-4}$	$1.2^{+1.7}_{-1.0}$	59.8	
		336	$\frac{7}{2}^+$	$(17^{+7}_{-10})\times10^{-3}$	$2.7^{+3.2}_{-2.7}$	40.2	795^{+410}_{-221}
		627	$\frac{5}{2}^+$				
		1085	$\frac{5}{2}^+$				
1307	$\frac{11}{2}^+$	0	$\frac{9}{2}^+$	$(44^{+8}_{-6})\times10^{-3}$	$0.43^{+0.28}_{-0.25}$	82	
		336	$\frac{7}{2}^+$		25 ± 5	18	250^{+400}_{-300}
		882	$\frac{13}{2}^+$				
1433	$\frac{5}{2}^+$	0	$\frac{9}{2}^+$		1.5 ± 0.03	2.3	
		336	$\frac{7}{2}^+$	0.18 ± 0.03	6.4–68	76.2	
		627	$\frac{5}{2}^+$			16.4	82^{+10}_{-8}
		928	$\frac{3}{2}^+$			1.9	
		1085	$\frac{5}{2}^+$			1.5	
		1179	$\frac{7}{2}^+$			1.7	

TABLE IV. (*Continued*)

Sussex				Yale			
*M*1 (W.u.)	*E*2 (W.u.)	Branch[b] (%)	T_m (fs)	*M*1 (W.u.)	*E*2 (W.u.)	Branch[b] (%)	T_m (fs)
1.69×10^{-2}	37.3	100	3.9×10^{4}	3.36×10^{-2}	36.3	100	2.2×10^{4}
	39.7	66.6			40.1	67.4	
			5371				5374
7.71×10^{-2}	22.8	33.4		7.50×10^{-2}	23.9	32.6	
	29.4	100	1970		28.7	100	2024
	32.4	91.2			32.4	90.6	
			1.2×10^{4}				1.2×10^{4}
6.07×10^{-4}	85.9	8.8		1.17×10^{-3}	86.2	9.4	
4.69×10^{-2}	9.9	97.1		6.88×10^{-2}	10.5	98.2	
			619				447
	13.1	2.4			10.3	1.4	
	11.3	3.2			10.6	3.1	
			7843				8062
3.25	0.152	96.8		3.16	8.77×10^{-2}	96.9	
	4.48×10^{-2}	0.1			2.09×10^{-2}	0.1	
0.131	1.72	97.2		0.111	1.49	99.3	
			549				661
1.58×10^{-2}	2.54×10^{-3}	2.6		6.07×10^{-4}	9.31×10^{-2}	0.1	
1.42×10^{-4}	5.8×10^{-4}	0		6.13×10^{-2}	0.122	0.5	
11×10^{-3}	1.03	56.5		0.175	9.45×10^{-3}	51.7	
5.12×10^{-3}	4.8×10^{-2}	8.5		0.239	6.22	26.3	
			866				56
67.8×10^{-3}	4.03	32.1		0.726	0.29	22	
1.23	0.202	2.8		1.71×10^{-2}	4.01	0.1	
5.34×10^{-3}	1.97	2.1		1.08×10^{-2}	2.13	4	
0.979	0.669	94.6	45	0.862	0.393	92.5	50
1.37	0.339	3.3		1.32	0.271	3.5	
6.77×10^{-2}	0.247	48.8		0.263	0.439	83.6	
0.167	1.70	48.4		0.112	6.37	15	
			107				47
1.55×10^{-2}	1.98	1.6		1.93×10^{-2}	4.03	0.9	
0.481	1.02	1.2		0.498	0.825	0.6	
74.3×10^{-3}	2.87	87.8		70.4×10^{-3}	1.66	87.8	
	18.9	8.2	156		20.5	9.6	168
9.67×10^{-2}	13.3	3.8		5.38×10^{-2}	7.84	2.3	
	0.197	0.1			0.231	0.1	
1.39	6.46	86.6		1.53	7.50	86.8	
0.131	2.25	3.3		0.278	1.35	6.2	
			15				13
1.33	0.846	8.1		0.892	1.92	4.9	
0.667	0.663	1.3		0.589	0.974	1.2	
0.257	9.99	0.2		1.15	2.62	0.8	

[a] Taken from Refs. 9 and 10.

[b] Except in cases where there is experimental evidence, calculated branching ratios of less than 1% are omitted.

counted for by the present calculation and in most cases there is a satisfactory agreement between experimental and theoretical excitation energies. It should be clarified at this point that the identification between theoretical and observed levels, indicated in Fig. 2, has not been made on energy grounds only but was based on the more sensitive criterion of transition rates. Thus the second $\frac{5}{2}+$ level observed[9,24] at 1085 keV has not been identified with the second theoretical $\frac{5}{2}+$ state but rather with the fourth since, as discussed below, such an identification ensures agreement with the observed decay rates of this level. A similar inversion occurs for the second $\frac{7}{2}+$ state observed at 1179 keV[9] which, in the case of the Sussex spectrum, is identified with the fourth theoretical $\frac{7}{2}+$ state. Taking these identifications into account, it may be observed from Fig. 2 that the Yale spectrum is in better agreement with experiment. Thus, the Sussex interaction accounts better for the observed excitation energies of levels below 1 MeV, but the spectrum obtained with this interaction becomes far too extended for energies higher than 1 MeV.

As may be seen from Fig. 2, the calculation predicts three states, namely: a third $\frac{9}{2}+$, a second $\frac{13}{2}+$, and a fourth $\frac{7}{2}+$ (second in the case of the Sussex interaction) for which no corresponding experimental levels have yet been observed. Evidence for a possible third $\frac{9}{2}+$ level at 1264 keV has been presented by Shibata, Itahashi, and Wakatsuki,[12] who studied the ^{93}Nb$(\alpha, 2n\gamma)^{95}$Tc reaction. However, the existence of this level has not been reconfirmed in the more recent experiment of Sarantites,[10] who studied the same reaction. In addition to the three mentioned states, the calculation predicts a low-lying $\frac{1}{2}+$ state. This state has been tentatively identified in Fig. 2 with the 1034 keV level which has spin $\frac{1}{2}$ (Ref. 9), but its parity has not yet been determined.

As expected, the wave functions of most of the low-lying states of ^{95}Tc are predominantly of $(0g_{9/2})^3(1d_{5/2})^2$ character. However, significant contributions arise from other neutron configurations and specially from those that contain the $2s_{1/2}$ orbital. These contributions are particularly pronounced in the case of the $\frac{5}{2}+$ states. Thus, the wave functions of the 627, 1085 and 1433 keV $\frac{5}{2}+$ states are found to contain about 50%, 70%, and 30%, respectively, admixtures of other than the $(0g_{9/2})^3(1d_{5/2})^2$ configurations. These results clearly justify the inclusion of all the neutron orbitals into the model space.

The theoretical predictions about the transition rates of the low-lying even-parity states of ^{95}Tc are compared with experiment in Table IV. In the calculation of $M1$ rates the bare $M1$ operator is used throughout this calculation. On the other hand, agreement with experiment on $E2$ rates can be obtained only through the introduction of effective charges. A common effective charge has been assigned to both protons and neutrons and this quantity has been treated as an adjustable parameter. It was found in this way that an effective charge of 1 produces best overall agreement with experiment.

The results contained in Table IV indicate that the two effective interactions employed in the calculation produce similar results on the transition rates of the low-lying states of ^{95}Tc except in the case of the second and third $\frac{7}{2}+$ states, where the results obtained with the Sussex interaction are in better agreement with experiment.

In the following we make individual comments about the decay of each level included in Table IV.

336 keV level. The multipole mixing ratio for the $\frac{7}{2}^+_1 \rightarrow$ g.s. transition has been measured recently. The values reported are -0.33 ± 0.06[9] and -0.37 ± 0.07 or $-3.8^{+0.8}_{-1.2}$.[10] Our results, which are -0.352 for the Yale interaction and -0.502 for the Sussex, are clearly in agreement with the smaller δ values. However, a complete comparison between theory and experiment cannot be made before the lifetime of the 336 keV level is established.

627, 882, 957, 1213, and 1307 keV levels. Table IV shows that the present calculation accounts satisfactorily for the observed decay of these five levels. However, it would be useful to known the lifetime of the 627 and 1213 keV levels since that would further check the predictions of the model.

928 keV level. Both Sussex and Yale calculations predict branching ratios that are not in agreement with experiment. This is due to the retarded $M1$ rate predicted by the model for the $\frac{3}{2}^+_1 \rightarrow \frac{5}{2}^+_1$ transition. On the other hand, the enhanced $E2$ rates predicted by the model seem to follow the experimental pattern.

1034 keV level. This is a possible $\frac{1}{2}+$ state.[9] However, no decay from this level to other positive-parity states has been observed so that the predictions of the model cannot be compared with experiment.

1085 keV level. The analysis of the ^{95}Mo $(p, n\gamma)$ ^{95}Tc experiment by Sarantites and Xenoulis[9] indicates with equal probability spin assignments of $\frac{5}{2}+$ and $\frac{7}{2}+$ for the 1085 keV level. However, a later experiment employing the same reaction[24] supports the $\frac{5}{2}+$ assignment which, for this reason, has been adopted here.

The calculation predicts three $\frac{5}{2}+$ levels in this energy region. From these the second and fourth (Fig. 2) fit satisfactorily the observed branching ratios of the 1085 keV level. However, if the sec-

ond $\frac{5}{2}+$ state is identified with the 1085 keV level, then the predicted lifetime is about 10 times faster from the experimental lower limit. For this reason the fourth $\frac{5}{2}+$ state has been adopted and the results of this identification, which are in very good agreement with experiment, are shown in Table IV.

1179 keV level. In the case of the Sussex interaction the fourth $\frac{7}{2}+$ state has been identified with the 1179 keV level, for similar reasons to those discussed in the case of the 1085 keV level. However, no similar identification is possible in the Yale case, since the calculated lifetime is about 6000 fs, which is in disagreement with the experimental estimate. For this reason the second $\frac{7}{2}+$ state of the Yale spectrum has been identified with the 1179 keV level. Such an identification ensures agreement with experiment on energies and branching ratios but not on lifetimes.

1281 and 1433 keV levels. From both theoretical spectra the third $\frac{7}{2}+$ state has been identified with the 1281 keV level and the second $\frac{5}{2}+$ with the 1433 keV level. Table IV shows that although the observed branching ratios are satisfactorily accounted for, the calculated lifetimes are faster than the experimental estimates.

B. Low-spin levels of ^{95}Tc between 1618 and 2324 keV

The ^{95}Mo$(p,n\gamma)^{95}$Tc reaction[9] has established the presence of twenty levels between 1618 and 2324 keV. These levels which have spins $\leq \frac{11}{2}$ are shown in Fig. 3. It may be seen from Fig. 3 that for most of the observed levels definite J^π assignments have not been made. In addition, the decay scheme of these levels is only partially known. The present calculation predicts many low-spin levels in this energy region. Thus, in addition to those states that have already been identified with experimental levels below 1433 keV the calculation predicts three $\frac{1}{2}+$, seven $\frac{3}{2}+$, nine $\frac{5}{2}+$, eleven $\frac{9}{2}+$, and eight $\frac{11}{2}+$ states between 1500 and 3100 keV excitation energy. Based on the existing experimental information, we have examined which of these theoretical states can be identified with experimental levels. As in Sec. III A the identification is attempted by requiring the agreement with experiment to be on the transition rates and not simply on the energies.

For five of the observed levels between 1618 and 2324 keV an identification with theoretical states is not possible. This is the case for the levels observed at 1639, 1694, 1920, 2210, and 2219 keV. The experimental data on the decay of these levels are so limited that they could be fitted by several of the theoretical stages that are close in energy to the corresponding observed levels. Moreover, no attempt has been made to identify any theoretical state with the 1618 keV level, since the latter is most probably[9] of negative parity.

The results of the calculation indicate that for the remaining 14 observed levels there exist theoretical states that have similar decay schemes. The calculated transition rates on which the identification between theoretical and observed levels has been based are given in Table V, while the identified theoretical levels are shown in Fig. 3.

Two general remarks should be made about the results shown in Table V. The first is that only transitions to levels below 1433 keV have been calculated. This is because there is no experimental information about transitions to levels above 1433 keV, and moreover there are uncertainties about the J^π values of these levels. The other remark

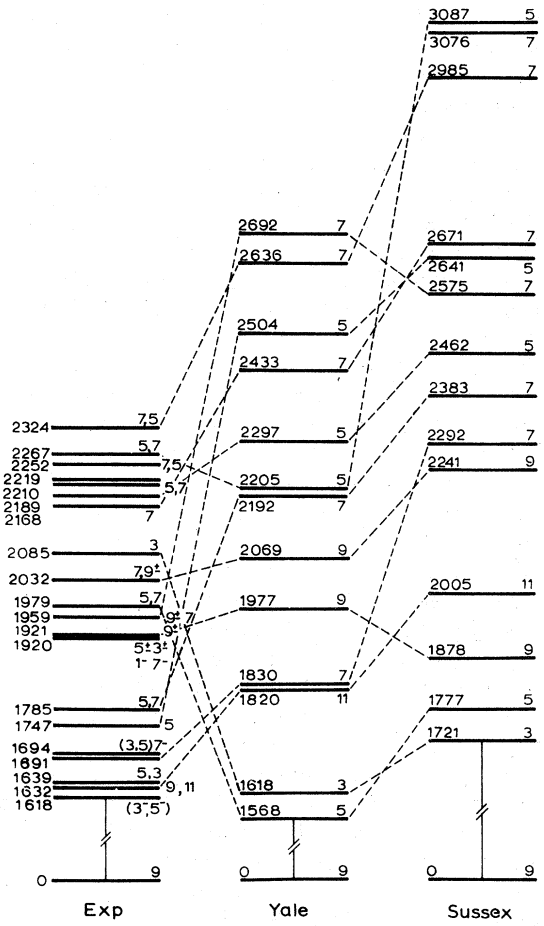

FIG. 3. The experimental (Ref. 9) and calculated low-spin even parity spectra of ^{95}Tc between 1618 and 2324 keV. The number on the right of each level corresponds to $2J$. Only those theoretical states that can be identified with observed levels (Sec. III B) are conveniently shown.

TABLE V. Experimental and calculated transition rates of the even-parity low-spin states of ^{95}Tc between 1632 and 2324 keV. Only transitions to states below 1433 keV have been calculated (see main text).

Initial state			Final state		Experiment[a]		Sussex				Yale			
E (keV)	Possible J^π	Assumed J^π	E (keV)	J^π	Branch (%)	T_m (fs)	$M1$ (W.u.)	$E2$ (W.u.)	Branch[b] (%)	T_m (fs)	$M1$ (W.u.)	$E2$ (W.u.)	Branch[b] (%)	T_m (fs)
1632	$\frac{9}{2}^+, \frac{11}{2}^+$	$\frac{11}{2}^+$	0	$\frac{9}{2}^+$	42		9.05×10^{-2}	0.163	48.5		6.84×10^{-2}	0.131	45.4	
			882	$\frac{13}{2}^+$	58	44^{+13}_{-9}	0.758	1.03	39.3	38	0.638	1.43	41	48
			957	$\frac{11}{2}^+$			0.179	4.09	6.8		0.219	2.5	10.3	
			1213	$\frac{9}{2}^+$			0.430	2.13	3.9		0.171	3.35	1.9	
1691	$\frac{5}{2}^+, \frac{7}{2}^+$	$\frac{7}{2}^+$	0	$\frac{9}{2}^+$	6.6		1.2×10^{-3}	0.464	2.4		3.54×10^{-3}	4.78×10^{-3}	2.8	
			336	$\frac{7}{2}^+$	48.4		0.16	2.86×10^{-2}	76.6		0.145	6.92×10^{-2}	58	
			627	$\frac{5}{2}^+$	39.5	120^{+35}_{-25}	7.44×10^{-2}	0.384	17.3	60	0.123	0.954	24	50
			1085	$\frac{5}{2}^+$			2.83×10^{-2}	6.22	1.3		0.292	4.37	10.5	
			1179	$\frac{7}{2}^+$			6.48×10^{-2}	0.747	1.7		5.82×10^{-2}	1.21	1.3	
			1213	$\frac{9}{2}^+$			1.03×10^{-2}	0.781	0.2		0.107	6.42×10^{-2}	1.9	
1747	$\frac{5}{2}^+$	$\frac{5}{2}^+$	0	$\frac{9}{2}^+$	0.6			2.44×10^{-3}	0			5.29×10^{-3}	0	
			336	$\frac{7}{2}^+$	63.8		0.151	0.902	70.8		8.7×10^{-2}	0.623	73.7	
			627	$\frac{5}{2}^+$	20.4		1.66×10^{-2}	0.835	4.1		3.04×10^{-2}	0.516	13	
			928	$\frac{3}{2}^+$	15.2	64^{+11}_{-9}	0.133	0.119	12.1	52	3.87×10^{-2}	5.06×10^{-3}	6.3	93
			1085	$\frac{5}{2}^+$			8.18×10^{-2}	7.67×10^{-3}	3.9		2.89×10^{-2}	0.53	2.5	
			1179	$\frac{7}{2}^+$			0.189	1.66	5.8		6.91×10^{-2}	1.42	3.8	
			1281	$\frac{7}{2}^+$			0.184	2.04	3.1		7.87×10^{-4}	0.836	0	
1785	$\frac{5}{2}^+, \frac{7}{2}^+$	$\frac{7}{2}^+$	0	$\frac{9}{2}^+$	50.1		2.43×10^{-2}	3.48×10^{-3}	44.5		7.38×10^{-2}	1.4×10^{-2}	64.9	
			336	$\frac{7}{2}^+$	9.8		1.64×10^{-2}	9.47×10^{-2}	16.3		2.34×10^{-2}	0.161	11.2	
			627	$\frac{5}{2}^+$	40.1	58^{+7}_{-6}	3.56×10^{-2}	0.204	17.9	101	7.95×10^{-2}	0.231	19.2	48
			1085	$\frac{5}{2}^+$			5.73×10^{-2}	0.123	4.1		1.27×10^{-4}	0.37	0	
			1179	$\frac{7}{2}^+$			8.98×10^{-2}	0.685	6.5		6.45×10^{-2}	0.442	2.2	
			1281	$\frac{7}{2}^+$			0.2	2.01	8.3		1.56×10^{-2}	2.08	0.3	
1921	$\frac{9}{2}^\pm$	$\frac{9}{2}^+$	0	$\frac{9}{2}^+$	23.9		7.11×10^{-2}	9.96×10^{-2}	20.3		2×10^{-2}	9.23×10^{-2}	7.5	
			336	$\frac{7}{2}^+$	76.1		0.369	0.489	59.1		0.326	0.149	67.2	
			627	$\frac{5}{2}^+$				8.97	1.3			7.33	1.4	

TABLE V. (*Continued*)

Initial state			Final state		Experiment [a]		Sussex				Yale			
E (keV)	Possible J^π	Assumed J^π	E (keV)	J^π	Branch (%)	T_m (fs)	$M1$ (W.u.)	$E2$ (W.u.)	Branch [b] (%)	T_m (fs)	$M1$ (W.u.)	$E2$ (W.u.)	Branch [b] (%)	T_m (fs)
			957	$\frac{11}{2}^+$		106^{+32}_{-22}	0.254	1.32	9.1	13	0.233	0.404	10.8	16
			1179	$\frac{7}{2}^+$			0.325	6.74×10^{-2}	5.3		0.391	0.353	8.3	
			1213	$\frac{9}{2}^+$			0.205	3.98	2.9		0.203	3.04	3.8	
			1281	$\frac{7}{2}^+$			0.124	0.655	1.3		1.25×10^{-2}	0.569	0.2	
1959	$\frac{9}{2}^\pm, \frac{7}{2}^+$	$\frac{7}{2}^+$	0	$\frac{9}{2}^+$	33.3		6.79×10^{-3}	6.73×10^{-2}	31.7		1.94×10^{-2}	7.34×10^{-2}	34	
			336	$\frac{7}{2}^+$	66.7		1.68×10^{-2}	0.261	44.8		5.92×10^{-2}	7.16×10^{-3}	58.1	
			627	$\frac{5}{2}^+$		$\geqslant 860$	3.97×10^{-3}	5.69×10^{-4}	5.6	188	4.46×10^{-3}	3.66×10^{-2}	2.5	72
			1085	$\frac{5}{2}^+$			2.6×10^{-4}	1.64	0.6		2.58×10^{-2}	0.126	4	
			1179	$\frac{7}{2}^+$			5.04×10^{-2}	1.16	14.5		6.14×10^{-3}	0.308	0.7	
1979	$\frac{5}{2}^+, \frac{7}{2}^+$	$\frac{5}{2}^+$	336	$\frac{7}{2}^+$	2.6		5.32×10^{-2}	0.826	14.3		4.21×10^{-2}	0.163	8.5	
			627	$\frac{5}{2}^+$	20.1		0.175	0.717	25.3		0.258	9.61×10^{-2}	29.1	
			928	$\frac{3}{2}^+$	66.6	57^{+13}_{-10}	0.528	8.33	36.4	18	0.9	5.8	47.5	14
			1085	$\frac{5}{2}^+$	10.7		0.459	1.14	19.2		8.78×10^{-2}	0.152	2.9	
			1179	$\frac{7}{2}^+$			3.96×10^{-2}	5.23	1.3		0.177	11.9	4.3	
			1281	$\frac{7}{2}^+$			0.155	0.368	3.1		0.46	3.04×10^{-4}	7.1	
2032	$\frac{7}{2}^+, \frac{9}{2}^\pm$	$\frac{9}{2}^+$	0	$\frac{9}{2}^+$	59		1.28×10^{-2}	0.906	43.3		9.9×10^{-2}	0.683	54.9	
			336	$\frac{7}{2}^+$	41		1.92×10^{-2}	3.95×10^{-2}	29.4		7.52×10^{-2}	2.04×10^{-2}	23.6	
			957	$\frac{11}{2}^+$		170^{+96}_{-50}	2.54×10^{-4}	3.04	1.5	98	1.02×10^{-2}	3.84	1.2	20
			1179	$\frac{7}{2}^+$			2.95×10^{-2}	1.08×10^{-2}	5.7		0.118	0.179	4.7	
			1281	$\frac{7}{2}^+$			9.26×10^{-2}	3.79×10^{-2}	12.2		1.81×10^{-2}	0.904	0.5	
			1307	$\frac{11}{2}^+$			5.54×10^{-2}	0.726	6.6		0.604	0.709	14.8	
2085	$\frac{3}{2}^+$	$\frac{3}{2}^+$	627	$\frac{5}{2}^+$	44.1		0.635	1.55	64.5		0.365	0.752	59.7	
			928	$\frac{3}{2}^+$	34.2		0.332	18.6	18.1		0.324	18.2	28.4	
			1034	$\frac{1}{2}^+$		53^{+25}_{-10}	9.9×10^{-2}	19.1	4.6	10	2.6×10^{-2}	17.8	2.8	16
			1085	$\frac{5}{2}^+$			0.304	6.24	10.1		4.22×10^{-3}	1.47	0.3	
			1433	$\frac{5}{2}^+$	21.7		5.36×10^{-3}	3.39×10^{-2}	0		0.505	1.56	7.4	
2168	$\frac{7}{2}^+$	$\frac{7}{2}^+$	0	$\frac{9}{2}^+$	1.8		1.66×10^{-3}	0.63	7.4		3.96×10^{-5}	0.638	6.1	

TABLE V. (*Continued*)

Initial state			Final state		Experiment[a]		Sussex				Yale			
E (keV)	Possible J^π	Assumed J^π	E (keV)	J^π	Branch (%)	T_m (fs)	$M1$ (W.u.)	$E2$ (W.u.)	Branch[b] (%)	T_m (fs)	$M1$ (W.u.)	$E2$ (W.u.)	Branch[b] (%)	T_m (fs)
			336	$\frac{7}{2}^+$	12.7		2.62×10^{-2}	6.18×10^{-2}	25.5		1.32×10^{-2}	3.33×10^{-2}	16.1	
			627	$\frac{5}{2}^+$	15.2		2.94×10^{-2}	0.477	17.5		3×10^{-2}	0.18	21.8	
			928	$\frac{3}{2}^+$	4.2			0.16	0.1			5.12×10^{-3}	0	
			1085	$\frac{5}{2}^+$		72^{+15}_{-12}	2.44×10^{-2}	0.338	5.4	49	2.37×10^{-4}	0.136	0.1	61
			1179	$\frac{7}{2}^+$	37.2		0.168	0.163	25.5		0.137	0.641	26	
			1213	$\frac{9}{2}^+$			2.16×10^{-3}	0.872	0.4		1.73×10^{-2}	0.777	3.1	
			1281	$\frac{7}{2}^+$			2.96×10^{-2}	0.815	3.3		4.15×10^{-2}	0.958	5.8	
			1433	$\frac{5}{2}^+$	28.9		0.223	0.216	14.6		0.265	0.433	20.6	
2189	$\frac{5}{2}^+, \frac{7}{2}^+$	$\frac{5}{2}^+$	0	$\frac{9}{2}^+$	2.5			0.799	4.4			0.238	1.6	
			336	$\frac{7}{2}^+$	7.8		1.68×10^{-2}	0.212	12.1		2.64×10^{-3}	0.265	3.1	
			627	$\frac{5}{2}^+$	5.7		4.29×10^{-2}	9.08×10^{-2}	17.8		7.55×10^{-3}	0.189	4.1	
			928	$\frac{3}{2}^+$	20.9		6.95×10^{-2}	9.16×10^{-2}	15.1		3.73×10^{-2}	0.165	10.1	
						53^{+17}_{-12}				34				42
			1085	$\frac{5}{2}^+$			4.33×10^{-2}	0.376	6.4		4.66×10^{-2}	1.82	8.8	
			1179	$\frac{7}{2}^+$	45.9		0.254	8.22×10^{-2}	28.4		0.353	0.806	49.1	
			1281	$\frac{7}{2}^+$			7.08×10^{-2}	4.16×10^{-2}	5.7		5.74×10^{-2}	6.5×10^{-2}	5.8	
			1433	$\frac{5}{2}^+$	17.2		0.208	0.656	9.8		0.291	8.2×10^{-2}	17.1	
2252	$\frac{7}{2}^+, \frac{5}{2}^+$	$\frac{7}{2}^+$	0	$\frac{9}{2}^+$	75.9		3.45×10^{-2}	4.27×10^{-2}	75.2					
			336	$\frac{7}{2}^+$			2.62×10^{-4}	0.683	3.7					
			627	$\frac{5}{2}^+$	20.5		1.34×10^{-2}	1.16×10^{-2}	11					
			928	$\frac{3}{2}^+$	3.6			0.505	0.4	59				
			1085	$\frac{5}{2}^+$			1.06×10^{-2}	5.42×10^{-2}	3.2					
			1179	$\frac{7}{2}^+$			4.12×10^{-3}	0.23	1					
			1213	$\frac{9}{2}^+$			2.3×10^{-2}	0.118	4.9					
2267	$\frac{5}{2}^+, \frac{7}{2}^+$	$\frac{5}{2}^+$	0	$\frac{9}{2}^+$	3.1			0.262	2.3			2.53×10^{-5}	0	
			336	$\frac{7}{2}^+$	22.2		1.44×10^{-2}	0.15	15.8		4.97×10^{-2}	0.533	24.6	
			627	$\frac{5}{2}^+$			4.2×10^{-3}	9.77×10^{-2}	2.9		9.26×10^{-3}	4.9×10^{-3}	2.7	
			928	$\frac{3}{2}^+$	20.1		1.22×10^{-2}	1.57×10^{-4}	4.3		3.12×10^{-2}	8.56×10^{-2}	5	

TABLE V. (*Continued*)

E_x (keV)	Initial state: Possible J^π	Initial state: Assumed J^π	Final state: E_x (keV)	Final state: J^π	Experiment[a]: Branch (%)	Experiment[a]: T_m (fs)	Sussex: $M1$ (W.u.)	Sussex: $E2$ (W.u.)	Sussex: Branch[b] (%)	Sussex: T_m (fs)	Yale: $M1$ (W.u.)	Yale: $E2$ (W.u.)	Yale: Branch[b] (%)	Yale: T_m (fs)
						315^{+750}_{-152}				46				21
			1085	$\frac{5}{2}^+$	27		0.179	9.47×10^{-2}	43.4		0.224	3.68	25	
			1179	$\frac{7}{2}^+$	27.6		0.133	0.1	25.2		0.438	1.28	37.5	
			1281	$\frac{7}{2}^+$			1.59×10^{-2}	0.167	2.3		5.82×10^{-2}	0.233	3.7	
			1433	$\frac{5}{2}^+$			4.29×10^{-2}	1.42×10^{-2}	3.7		3.59×10^{-2}	0.724	1.4	
2324	$\frac{7}{2}^+, \frac{5}{2}^+$	$\frac{7}{2}^+$	0	$\frac{9}{2}^+$	63.1		9.96×10^{-2}	0.19	65.8		1.91×10^{-2}	2.93×10^{-2}	47	
			336	$\frac{7}{2}^+$	31.3		5.05×10^{-2}	2.02×10^{-2}	20.7		1.2×10^{-2}	0.468	21.2	
			627	$\frac{5}{2}^+$	5.6		8.92×10^{-3}	0.143	2.4		7.38×10^{-3}	6.15×10^{-3}	7	
			1085	$\frac{5}{2}^+$			9.26×10^{-2}	6.56×10^{-2}	9.2	16	2.52×10^{-3}	9.41×10^{-3}	9.3	61
			1179	$\frac{7}{2}^+$			1.9×10^{-3}	1.16	0.3		3.68×10^{-2}	0.778	11	
			1281	$\frac{7}{2}^+$			2.36×10^{-3}	0.204	1.4		3.22×10^{-3}	2.38×10^{-2}	0.7	
			1433	$\frac{5}{2}^+$			8.69×10^{-3}	1.74×10^{-3}	0.1		1.74×10^{-2}	0.702	2.5	

[a] Reference 9.

[b] Except in cases where there is experimental evidence, calculated branching ratios of less than 1% are omitted.

is that since the present calculation is limited to the even-parity states of ^{95}Tc, all the experimental states included in Table V have been assumed to be of positive parity. However, from the existing experimental information,[9] the negative-parity assignment cannot be excluded from the levels observed at 1921, 1959, and 2032 keV.

Table V shows that if the levels at 1921 and 2032 keV are of positive parity, then their decay can be accounted by the present calculation, provided both these levels have spin $\frac{9}{2}$. Similarly, the 1959 keV level can be interpreted as a $\frac{7}{2}+$ state provided its lifetime is found to be close to the lower limit set by Sarantites and Xenoulis.[9] It should be remembered that the J^π values of these three levels, adopted here, are not experimentally excluded.

For three of the experimental levels, namely those observed at 1747, 2085 and 2168 keV, definite J^π values have been established. Table V shows that the theoretical predictions regarding the decay of these three levels are in satisfactory agreement with experiment. Three $B(M1)$ strengths have been estimated by Sarantites and Xenoulis[9] from the decay of the 1747 keV level. These $B(M1)$ values are 0.111, 7.11×10^{-2}, and 0.135 Weisskopf units (W.u.) for the 1747→336, 1747→627, and 1747→928 transitions, respectively. [These values are quoted wrongly in Ref. 9. The correct values (listed in the text) have been communicated to us by Xenoulis.] Table V shows that the model reproduces very satisfactorily these three $B(M1)$ values. On these grounds the identification of the 1747 keV level with the theoretical states that are indicated in Fig. 3 becomes unambiguous despite the fact that in the theoretical spectra there exist other $\frac{5}{2}+$ states which are closer in energy to the observed level.

There are certain experimental states that can be understood in terms of this calculation only if they are found to have the spin assignments indicated in Table V. Thus, the present model cannot explain the strong branch to the ground state observed in the decay of the 1785, 2252, and 2324 keV levels, unless these states are $\frac{7}{2}+$, a possibility which, although not unique, is suggested by the experiment as well. The other possible J^π assignment for these three levels, namely the $\frac{5}{2}+$, would require a very enhanced $E2$ rate to the ground state which this calculation does not predict. Similarly, the strong branch to the $\frac{3}{2}+$ at 928 keV observed in the decay of the 1979, 2189 and 2267 keV levels can be predicted by the present calculation only if these three levels are $\frac{5}{2}+$ states, a possibility which, again, is not experimentally excluded. In the same category one can classify the 1632 keV level for which the proposed J^π val-

ues[9] are $\frac{9}{2}+$ and $\frac{11}{2}+$. The present calculation does not predict a $\frac{9}{2}+$ state that could fit the observed decay scheme of the 1632 keV level. In particular, with a $J^\pi = \frac{9}{2}+$ is not possible to account for the very enhanced $B(E2)$ value which is necessary in order to explain the 58% branch to the $\frac{13}{2}+$ state at 882 keV. On the other hand, identification of the 1632 keV level with the third theoretical $\frac{11}{2}+$ state results, as Table V shows, in very good agreement with experiment. This is further demonstrated by the agreement between the theoretical and the measured $B(M1)$ value (6.8×10^{-2} W.u.) (value estimated by Sarantites and Xenoulis[9] on the assumption that the 1632 keV level is $\frac{11}{2}+$) in the 1632 → g.s. transition.

It may be seen from Table V that the 2252 keV level is identified with a theoretical state in the case of the Sussex interaction but not in the case of the Yale. The existing information[9] on the 2252 keV level suggests that the 2252 → 336 branch is small, a feature that cannot be accounted for by any of the $\frac{7}{2}+$ states obtained with the Yale interaction. Apart from the 2252 keV level it may be seen from Table V that the transition rates obtained with the Sussex interaction are generally in better agreement with experiment. This is not the case with the excitation energy (Fig. 3), where the more compressed Yale spectrum is in much better agreement with experiment. However, before conclusions can be drawn about which of the two interactions is the most appropriate for ^{95}Tc, more definite experimental information is required so that the identification attempted here can become unambiguous.

C. High-spin levels of ^{95}Tc

The ^{93}Nb$(\alpha, 2n\gamma)^{95}$Tc reaction[10-12] has established the presence of several levels that have $J^\pi \geq \frac{15}{2}$ between 1515 and 5604 keV. Many high-spin levels are predicted by the present calculation in this energy region. The calculated excitation energies of few of the lowest states for each J^π value are listed in Table VI for the case of the Sussex interaction, while similar results have been obtained with the Yale interaction. Figure 4 shows those theoretical states that can be identified, on the basis of similar decay properties, with observed levels. The theoretical predictions on the transition rates of the high-spin levels of ^{95}Tc are compared with experiment in Table VII.

It may be seen from Table VII that the theoretical predictions on the decay of the high-spin levels of ^{95}Tc are in satisfactory agreement with experiment.[10] This agreement is also extended to the energy spectrum where, as Fig. 4 shows, the calculated excitation energies are quite close to the experimental values. The only exception to this agreement is presented in the case of the first two $\frac{19}{2}^+$ states. Figure 4 shows that the theoretical first and second $\frac{19}{2}^+$ states appear quite close in energy to the corresponding observed levels. In order, however, to obtain agreement with experiment on transition rates we found necessary to identify the lowest theoretical $\frac{19}{2}^+$ with the second experimental and vice versa. This point is further discussed below, together with some other general comments about the results of the calculation on the high-spin levels of ^{95}Tc.

$\frac{15}{2}+$ and $\frac{17}{2}+$ states. As Fig. 4 and Table VII indicate, the present calculation accounts satisfactorily for the energies and transition rates of the two $\frac{15}{2}+$ levels observed at 1549 and 2119 keV and of the two $\frac{17}{2}+$ states at 1515 and 2231 keV. There are two more possible $\frac{17}{2}+$ levels at 3038 and 3065 keV. As Table VI shows, there are several theoretical $\frac{17}{2}+$ states in this energy region. However, no experimental information is available on the decay of the 3065 keV level so an identification with theoretical states is not possible. On the other hand, the observed decay of the 3038 keV level can be accounted by this model only if this level is a $\frac{19}{2}+$, which is not experimentally excluded.

The 50% branch to the $\frac{11}{2}+$ at 957 keV which has been observed in the decay of the $\frac{15}{2}+$ state at 1549 keV is underestimated in the results of the present calculation. This strong branch is due either to a very fast $E2$ rate in the 1549 → 957 transition, or to a retarded $M1$ rate in the 1549 → 882 transition. Before the lifetime of the 1549 keV level is precisely measured one cannot decide in which direction the present results ought to be improved.

$\frac{19}{2}+$ levels. Two $\frac{19}{2}+$ levels at 2183 and 2906 keV have been observed in the ^{93}Nb$(\alpha, 2n\gamma)^{95}$Tc experiment.[10] As Table VII shows, the experimental data on the 2906 keV level indicate a very retarded $M1$ rate to the $\frac{17}{2}+$ level at 1515 keV. Among the theoretical $\frac{19}{2}+$ states only the lowest could reasonably reproduce the observed decay of the 2906 keV level and, for this reason, such an identification has been adopted. On the other hand, the second theoretical $\frac{19}{2}+$ state has been identified with the 2183 keV level for two reasons. First, because this is the best choice on energy grounds and second, because transitions of higher levels to the 2183 keV state are in this way better reproduced. As seen from Table VII, the model fails to explain the observed branching ratios in the decay of the 2183 keV level. Since our results regarding the 2183 → 1515 transition are in very good agreement with experiment, this failure is entirely due to the inability of the model to reproduce the extreme enhancement of the $E2$ rate

TABLE VI. Excitation energies (measured in keV) of the high-spin states of ^{95}Tc calculated with the Sussex interaction.

$E_{15/2}$	$E_{17/2}$	$E_{19/2}$	$E_{21/2}$	$E_{23/2}$	$E_{25/2}$	$E_{27/2}$	$E_{29/2}$	$E_{31/2}$	$E_{33/2}$
1474	1330	2400	2453	3677	3498	4481	4120	6154	5752
2015	2275	3033	3125	4040	4379	5306	5359	6465	8739
2498	2846	3263	3346	4368	4645	5618	6251	...	
2671	3042	3557	3828	4563	4772	5972	6626		
2728	3286	3715	4060	4927	5303	6041	6794		
2947	3343	3923	4286	4955	5665	...	...		
3147	3514	4038	4483	5172	5752				
3181	3549	4091	4698	5461	6109				
...	...	...	...	...	...				

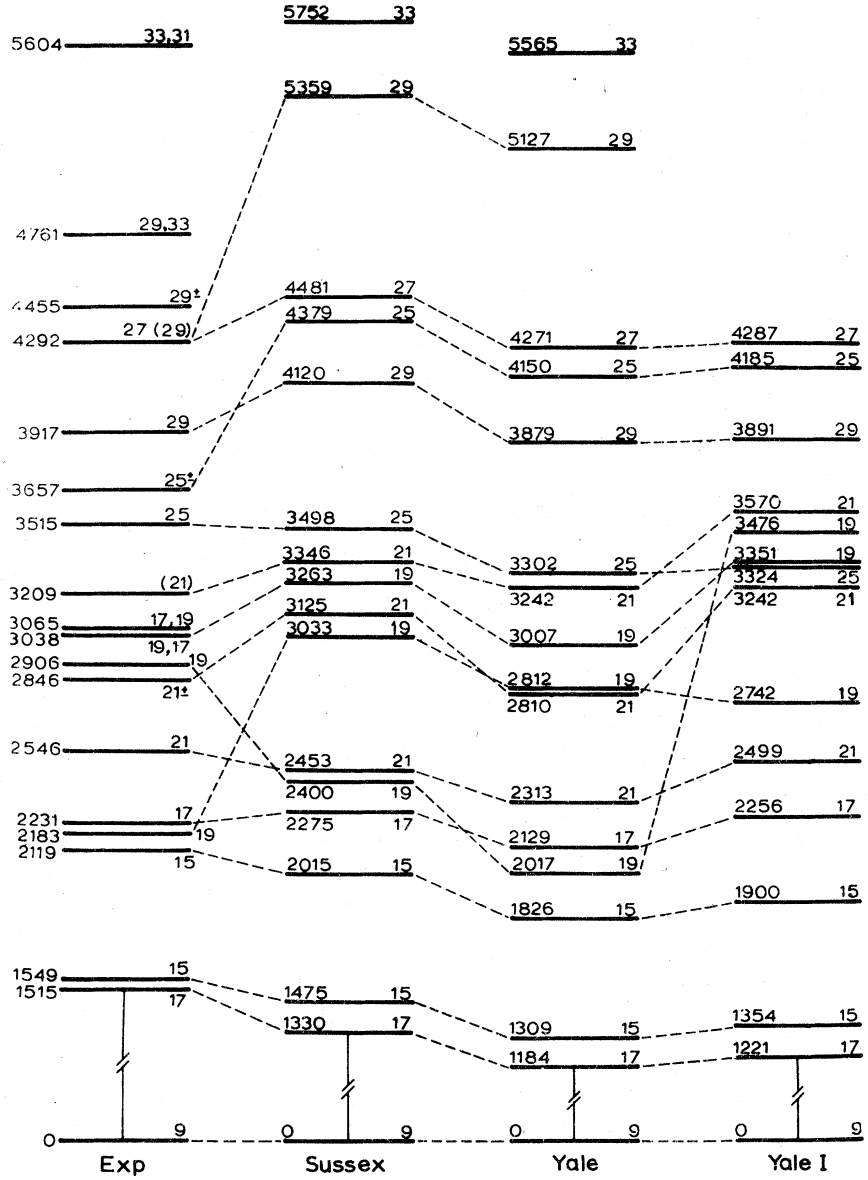

FIG. 4. The experimental (Refs. 10–12) and calculated high-spin ($2J \geq 15$) even parity states of ^{95}Tc. The spectrum Yale 1 has been obtained with an $\epsilon g_{7/2}$ value of 4.25 MeV (Sec. III D).

TABLE VII. Experimental and calculated transition rates of the high-spin even-parity states of ^{95}Tc.

Initial state		Final state		Experiment[a]			
E (keV)	J^π	E (keV)	J^π	$M1$ (W.u.)	$E2$ (W.u.)	Branch (%)	T_m (fs)
1515	$\frac{17}{2}^+$	882	$\frac{13}{2}^+$			100	
1549	$\frac{15}{2}^+$	882	$\frac{13}{2}^+$	≤ 0.02	≤ 29	50	
							>2000
		957	$\frac{11}{2}^+$		≤ 110	50	
2119	$\frac{15}{2}^+$	882	$\frac{13}{2}^+$	$(48 \pm 12) \times 10^{-3}$	0.06–0.66	83	
		1307	$\frac{11}{2}^+$				290^{+90}_{-60}
		1515	$\frac{17}{2}^+$	$(84 \pm 21) \times 10^{-3}$		17	
2183	$\frac{19}{2}^+$	1515	$\frac{17}{2}^+$	$(38^{+26}_{-16}) \times 10^{-3}$	$6.8^{+4.8}_{-3.8}$	47	
							1200^{+1300}_{-600}
		1549	$\frac{15}{2}^+$		130^{+100}_{-53}	53	
2231	$\frac{17}{2}^+$	882	$\frac{13}{2}^+$		2.4 ± 1.3	5	
		1515	$\frac{17}{2}^+$	$0.48^{+0.21}_{-0.11}$	≤ 65	85	150 ± 40
		1549	$\frac{15}{2}^+$	$(67^{+31}_{-24}) \times 10^{-3}$	c	10	
2546	$\frac{21}{2}^+$	1515	$\frac{17}{2}^+$		$3.2^{+1.6}_{-1.3}$	35	
							3000^{+2000}_{-1000}
		2183	$\frac{19}{2}^+$	$0.14^{+0.07}_{-0.06}$	0.7–7.1	65	
2847	$\frac{21}{2}^+$	1515	$\frac{17}{2}^+$				
		2183	$\frac{19}{2}^+$	≤ 0.05	≤ 0.15	100	>3000
		2546	$\frac{21}{2}^+$				
2906	$\frac{19}{2}^+$	1515	$\frac{17}{2}^+$	$(44 \pm 20) \times 10^{-5}$	c	1.5	
		1549	$\frac{15}{2}^+$		$1.7^{+0.8}_{-0.6}$	10	
		2119	$\frac{15}{2}^+$				
							400 ± 100
		2183	$\frac{19}{2}^+$	$(39^{+13}_{-10}) \times 10^{-3}$	125^{+61}_{-44}	51	
		2231	$\frac{17}{2}^+$	$\leq 9.1 \times 10^{-3}$	c	≤ 3.5	
		2546	$\frac{21}{2}^+$	$0.53^{+0.14}_{-0.09}$	240^{+150}_{-120}	33	
3038	$\frac{19}{2}^+$	1515	$\frac{17}{2}^+$	$(20^{+7}_{-5}) \times 10^{-3}$	$0.27^{+0.17}_{-0.10}$	61	
		1549	$\frac{15}{2}^+$				
		2119	$\frac{15}{2}^+$				
							270^{+30}_{-70}
		2231	$\frac{17}{2}^+$				
		2546	$\frac{21}{2}^+$	$0.38^{+0.13}_{-0.06}$	c	39	
		2847	$\frac{21}{2}^+$				
3209	$\frac{21}{2}^+$	1515	$\frac{17}{2}^+$		$4.1^{+0.9}_{-0.5}$	100	
		2183	$\frac{19}{2}^+$				
							550^{+80}_{-100}
		2546	$\frac{21}{2}^+$				
		2847	$\frac{21}{2}^+$				
3515	$\frac{25}{2}^+$	2546	$\frac{21}{2}^+$		≤ 5.3	100	
							>7000
		2847	$\frac{21}{2}^+$				
3657	$\frac{25}{2}^+$	2546	$\frac{21}{2}^+$				
		2847	$\frac{21}{2}^+$				

TABLE VII. (*Continued*)

Sussex				Yale			
$M1$ (W.u.)	$E2$ (W.u.)	Branch[b] (%)	T_m (fs)	$M1$ (W.u)	$E2$ (W.u)	Branch[b] (%)	T_m (fs)
	25.4	100	1.2×10^4		23.6	100	1.3×10^4
1.94×10^{-2}	2.41	81.2		3.43×10^{-2}	2.37	89.2	
			4194				2667
	18.5	18.2			16.6	10.4	
0.123	0.646	79.7		0.116	0.318	82.2	
	16.4	1.9	102		17	2.3	117
0.238	9.35	17.3		0.176	0.91	14.8	
59.8×10^{-3}	2.24	98.6		47.2×10^{-3}	2.87	97.7	
			1705				2119
	2.48	1.4			3.24	2.3	
	7.42	5.5			8.35	7.6	
1.46	3.02×10^{-2}	87.5	51	1.16	4.68×10^{-2}	85.9	63
0.135	0.126	7		0.1	7.04×10^{-3}	6.4	
	17.6	71.8			15.5	69	
			1084				1181
0.17	1.18	28.1		0.171	1.67	30.8	
	0.914	1.9			3.07	7.1	
0.642	3.73	94.6	157	0.566	3.91	90.1	170
0.252	0.741	3.5		0.191	0.909	2.8	
99.4×10^{-5}	2.89×10^{-4}	2.7		17.3×10^{-5}	2.06×10^{-2}	0.9	
	9.15	42.5			6.86	49.2	
	2.28	0.7			3.68	1.7	
			313				483
87.4×10^{-3}	3.67	33.6		34.5×10^{-3}	0.826	20.4	
5.04×10^{-3}	1.27	1.7		2.09×10^{-3}	0.552	1.1	
0.402	4.28	18.8		0.37	4.95	26.6	
27.1×10^{-3}	1.36	43.8		25.9×10^{-3}	0.767	41.9	
	1.9	5.8			3.35	10.6	
	8.39	2.3			6.88	2	
			128				134
0.159	0.174	34.3		0.142	0.328	32	
0.256	0.812	12.5		0.233	0.734	11.9	
0.206	0.21	0.6		0.54	0.348	1.6	
	4.21	6			2.44	4.6	
0.307	0.668	33.7		0.155	0.474	22.7	
			32				42
1.95	0.551	57.7		1.75	0.386	69	
0.454	0.553	2.2		0.5	0.642	3.2	
	17.6	96.6			14.1	92.4	
			1987				2371
	3.96	3.4			7.51	7.6	
	0.162	6.5			0.505	17.3	
	1.67	13.8	7334		1.96	13.8	6279

TABLE VII. (*Continued*)

Initial state E (keV)	Initial state J^π	Final state E (keV)	Final state J^π	Experiment[a] $M1$ (W.u.)	Experiment[a] $E2$ (W.u.)	Experiment[a] Branch (%)	Experiment[a] T_m (fs)
		3515	$\frac{25}{2}^+$				
3917	$\frac{29}{2}^+$	3515	$\frac{25}{2}^+$			100	
4292	$\frac{27}{2}^+$	3515	$\frac{25}{2}^+$				
		3657	$\frac{25}{2}^+$				
		3917	$\frac{29}{2}^+$				
4292	$\frac{29}{2}^+$	3515	$\frac{25}{2}^+$				
		3657	$\frac{25}{2}^+$				
		3917	$\frac{29}{2}^+$			100	

observed in the 2183 → 1549 transition.

The state observed at 3038 keV has possible J^π values of $\frac{19}{2}+$ and $\frac{17}{2}+$.[10] The observed strong branch to the $\frac{21}{2}+$ state at 2546 keV cannot be explained by the present calculation if the 3038 keV level is a $\frac{17}{2}+$ state. On the other hand, identification of the third theoretical $\frac{19}{2}+$ state with the 3038 keV level explains, as Table VII shows, satisfactorily the observed decay of this level.

$\frac{21}{2}+$ states. The analysis of the ^{93}Nb$(\alpha, 2n\gamma)^{95}$Tc experiment[10,12] has established that the first $\frac{21}{2}+$ state of ^{95}Tc appears at 2546 keV. Moreover, the existing information[10] suggests that the levels observed at 2847 and 3209 keV might also be $\frac{21}{2}+$ states. These levels have been identified with the three lowest theoretical $\frac{21}{2}+$ states.

Table VII shows that the 2546 keV level could be identified with each of the three $\frac{21}{2}+$ states, as a comparison between experimental and theoretical $B(M1)$ and $B(E2)$ values indicates. The identification of the first theoretical $\frac{21}{2}+$ state with the 2546 keV level, ensures, however, better agreement with experiment on the cascade $\frac{29}{2}^+_1 \rightarrow \frac{25}{2}^+_1 \rightarrow \frac{21}{2}^+_1$.

On the assumption that the 2847 keV level has positive parity, we have identified it with the second theoretical $\frac{21}{2}+$ state. This identification accounts, as Table VII shows, for the observed branching ratios of the 2847 keV level. However, the calculated lifetime is about 20 times faster than the experimentally set lower limit, a fact which makes doubtful such an identification.

As Table VII shows, the model fails completely to account for the decay of the 3209 keV level. If this level is found to be a $\frac{21}{2}+$ state, then it must belong to configurations other than those considered in the present calculation.

Levels observed above 3515 keV. The analysis of the ^{93}Nb$(\alpha, 2n\gamma)^{95}$Tc reaction [10,11] has established spins of $\frac{25}{2}+$ and $\frac{29}{2}+$ for the 3515 and 3917 keV levels, respectively. Moreover, the 3657 keV level has been found to be a $\frac{25}{2}$ state but its parity has not yet been established. The calculation predicts two $\frac{25}{2}+$ states that are close in energy to the two observed levels. Since the $B(E2)$ value corresponding to the 3515 → 2546 transition is only approximately known, it is difficult to decide which of the two theoretical $\frac{25}{2}+$ states ought to be identified with the 3515 keV level. However, the identification of the first theoretical $\frac{25}{2}+$ state with the 3515 keV level ensures agreement with experiment on the cascade $\frac{29}{2}^+_1 \rightarrow \frac{25}{2}^+_1 \rightarrow \frac{21}{2}^+_1$, as Table VII shows.

The only information available about the 3657 keV level is that it decays with a 100% branch to the 2847 keV level. On the assumption that both the 2847 and 3657 keV levels have positive parity, we have identified the second theoretical $\frac{25}{2}+$ state with the 3657 keV level and calculated its decay. The results, shown in Table VII, are not in agreement with experiment. Thus, even if one assumes that, due to the proximity of the 3515 and 3657 keV levels, the γ rays corresponding to that transition have not been observed, still one can see from Table VII that the model predicts about equal intensities for the 3657 → 2546 and 3657 → 2847 transitions.

The level observed at 4292 keV seems to be the first $\frac{27}{2}+$ state of ^{95}Tc, although the $\frac{29}{2}+$ assignment cannot be excluded.[10] Table VII shows that the observed branching ratios in the decay of the 4292 keV level can be better reproduced if this level is identified with the second theoretical $\frac{29}{2}+$ state, rather than with the lowest $\frac{27}{2}+$ state. Against, however, such an identification is the difference between calculated and experimental excitation energy.

Apart from excitation energy and possible J^π values, very little is known for the states higher than 4292 keV. For this reason no identification

TABLE VII. (*Continued*)

Sussex				Yale			
$M1$ (W.u.)	$E2$ (W.u.)	Branch[b] (%)	T_m (fs)	$M1$ (W.u.)	$E2$ (W.u.)	Branch[b] (%)	T_m (fs)
1.19	0.886	79.7		1.2	0.835	68.8	
	11.6	99.1	2.5×10^5		11.3	100	2.6×10^5
0.148	0.202	23.6		0.113	0.105	18.6	
0.481	1.27	41.6	106	0.513	1.25	46.1	110
1.95	0.113	37.4		1.91	0.188	35.3	
	2.4	6.4			1.98	8.2	
	1.41	1.4	2930		1.81	2.8	4523
0.187	0.206	92.2		0.117	0.115	89	

[a]Reference 10.
[b]Calculated branching ratios of less than 1% are omitted.
[c]Assumed to be pure $M1$ transition (Ref. 10).

of theoretical with experimental states can be attempted. However, it is quite possible that the model fails at such high excitation energies. This is evidenced by the presence in the experimental spectrum of three possible $\frac{29}{2}+$ states above 4292 keV, while the model can account for only one. It is very probable, therefore, that at such high excitation energies configurations other than those considered here play an important role.

D. Use of a different single-particle spectrum

Most of the high-spin levels that have been identified with observed levels (Sec. III C) have been found to belong predominantly to the $(0g_{9/2})^3$-$(1d_{5/2})^2$ configurations. There are, however, some significant exceptions to that rule. Thus the wave function of the lowest $\frac{19}{2}+$ state contains about 90% admixtures of $(0g_{9/2})^3(1d_{5/2}0g_{7/2})$ components. Moreover, the wave functions of the first two $\frac{21}{2}+$ states are composed of about equal mixtures of $(0g_{9/2})^3(1d_{5/2})^2$ and $(0g_{9/2})^3(1d_{5/2}0g_{7/2})$ components. These results indicate that the excitation energies of these three states and in particular of the lowest $\frac{19}{2}+$ state are sensitive functions of the $0g_{7/2}$ single-particle energy. Thus, one expects that a larger value of $\epsilon g_{7/2}$ than the one adopted in (3) will improve agreement with experiment with respect to the excitation energies of the $\frac{19}{2}+$ states. In the following we examine the effects which an increase of the $\epsilon g_{7/2}$ from 3.0 to 4.25 MeV has on the energy spectrum and the transition rates of the high-spin levels of ^{95}Tc.

The energy spectrum of the high-spin levels of ^{95}Tc corresponding to an $\epsilon g_{7/2}$ value of 4.25 MeV is shown in Fig. 4. Since, as shown in Sec. III C, the Sussex and Yale interactions produce very similar results on the high-spin levels of ^{95}Tc, this new calculation has been performed only with the Yale interaction. Figure 4 shows that the energies of most of the high-spin states are only slightly affected by the increase in the $\epsilon g_{7/2}$ value. This can be easily understood by the fact that the wave functions of these states contain only small $g_{7/2}$ admixtures. On the other hand, Fig. 4 shows that the inversion of the lowest two $\frac{19}{2}+$ states, which has been observed with the single-particle spectrum (3), has now been corrected.

The effects on transition rates produced by the change in the $\epsilon g_{7/2}$ energy are presented in Table VIII. Due to the very small $0g_{7/2}$ admixtures in the wave functions of the states below 2183 keV, there are no significant differences in the results with the two different $\epsilon g_{7/2}$ values. Therefore, the decay of the states below 2183 keV has been conveniently omitted from Table VIII.

In contrast to the energy spectrum, the results of Table VIII suggest that the increase of $\epsilon g_{7/2}$ from 3.0 to 4.25 MeV does not, in general, improve agreement with experiment on transition rates. This is evidenced even in the decay of the 2546 keV level, where the branching ratios that have been obtained with the new $\epsilon g_{7/2}$ value appear to be in excellent agreement with experiment. However, an inspection of the matrix elements, shown in Table VIII, reveals that this improvement is due to an increase of the $M1$ rate in the 2546 → 2183 decay, which is not justified by the experimental data. Similar cases can be found in the decay of the 2906 and 3038 keV levels where an examination of the $B(M1)$ values favors the predictions of the calculation with the original single-particle spectrum (3). For these reasons the use of an $\epsilon g_{7/2}$ value of 4.25 MeV has not been adopted for the rest of the calculation.

TABLE VIII. Dependence of the transition rates of the high-spin states of ^{95}Tc on the $0g_{7/2}$ neutron single-particle energy.

Initial state		Final state		Experiment[a]				Yale[b]				Yale I[c]			
E (keV)	J^π	E (keV)	J^π	$M1$ (W.u.)	$E2$ (W.u)	Branch (%)	T_m (fs)	$M1$ (W.u.)	$E2$ (W.u.)	Branch[d] (%)	T_m (fs)	$M1$ (W.u.)	$E2$ (W.u.)	Branch[d] (%)	T_m (fs)
2183	$\frac{19}{2}^+$	1515	$\frac{17}{2}^+$	$(38^{+26}_{-16})\times10^{-3}$	$6.8^{+4.8}_{-3.8}$	47	1200^{+1300}_{-600}	47.2×10^{-3}	2.87	97.7	2119	50.3×10^{-3}	1.75	94.7	1949
		1549	$\frac{15}{2}^+$		130^{+100}_{-53}	53			3.24	2.3			8.19	5.3	
2546	$\frac{21}{2}^+$	1515	$\frac{17}{2}^+$		$3.2^{+1.6}_{-1.3}$	35	3000^{+2000}_{-1000}		15.5	69	1181		17.1	34.5	539
		2183	$\frac{19}{2}^+$	$0.14^{+0.07}_{-0.06}$	0.7–7.1	65		0.171	1.67	30.8		0.795	4.86	65.4	
2847	$\frac{21}{2}^+$	1515	$\frac{17}{2}^+$					3.07	7.1				2.21	6.5	
		2183	$\frac{19}{2}^+$	≤0.05	≤0.15	100	>3000	0.566	3.91	90.1	170	0.256	0.305	52.1	218
		2546	$\frac{21}{2}^+$					0.191	0.909	2.8		2.17	1.61	41.3	
2906	$\frac{19}{2}^+$	1515	$\frac{17}{2}^+$	$(44\pm20)\times10^{-5}$	e	1.5		17.3×10^{-5}	2.06×10^{-2}	0.9		162×10^{-5}	3.35×10^{-2}	5	
		1549	$\frac{15}{2}^+$		$1.7^{+0.8}_{-0.6}$	10			6.86	49.2			6.65×10^{-2}	0.3	
		2119	$\frac{15}{2}^+$				400 ± 100		3.68	1.7	483		2.43×10^{-2}	0	345
		2183	$\frac{19}{2}^+$	$(39^{+13}_{-10})\times10^{-3}$	125^{+61}_{-44}	51		34.5×10^{-3}	0.826	20.4		198×10^{-3}	0.253	82.2	
		2231	$\frac{17}{2}^+$	$\leq9.1\times10^{-3}$	e	≤3.5		2.09×10^{-3}	0.552	1.1		2.96×10^{-2}	0.159	10	
		2546	$\frac{21}{2}^+$	$0.53^{+0.14}_{-0.09}$	240^{+150}_{-120}	33		0.37	4.95	26.7		4.69×10^{-2}	2.78×10^{-2}	2.4	
3038	$\frac{19}{2}^+$	1515	$\frac{17}{2}^+$	$(20^{+7}_{-5})\times10^{-3}$	$0.27^{+0.17}_{-0.10}$	61		25.9×10^{-3}	0.767	41.9		13.1×10^{-3}	0.576	60.1	
		1549	$\frac{15}{2}^+$						3.35	10.6			3.22×10^{-2}	0.3	
		2119	$\frac{15}{2}^+$						6.88	2			1.61	1.3	
		2183	$\frac{19}{2}^+$				270^{+30}_{-70}	8.28×10^{-7}	0.165	0	134	3.92×10^{-2}	3.76	30.8	368
		2231	$\frac{17}{2}^+$					0.142	0.328	32		2.66×10^{-3}	0.496	1.8	
		2546	$\frac{21}{2}^+$	$0.38^{+0.13}_{-0.06}$	e	39		0.233	0.734	11.9		2.31×10^{-2}	1.39	3.2	
		2847	$\frac{21}{2}^+$					0.54	0.348	1.6		0.308	1.11	2.5	
3515	$\frac{25}{2}^+$	2546	$\frac{21}{2}^+$		≤5.3	100	>7000		14.1	92.4	2371		20.1	99.8	1800
		2847	$\frac{21}{2}^+$						7.51	7.6			0.3	0.2	
3657	$\frac{25}{2}^+$	2546	$\frac{21}{2}^+$						0.505	16.9			0.44	1.2	
		2847	$\frac{21}{2}^+$			100			1.96	13.5	6131		8.26	44.8	4821
		3515	$\frac{25}{2}^+$					1.2	0.835	67.2		1.23	0.71	54	

TABLE VIII. (*Continued*)

Initial state E (keV)	J^π	Final state E (keV)	J^π	$M1$ (W.u.)	Experiment[a] $E2$ (W.u)	Branch (%)	T_m (fs)	$M1$ (W.u.)	Yale[b] $E2$ (W.u)	Branch[d] (%)	T_m (fs)	$M1$ (W.u.)	Yale I[c] $E2$ (W.u)	Branch[d] (%)	T_m (fs)
3917	$\frac{29^+}{2}$	3515	$\frac{25^+}{2}$			100			11.3	100	2.6×10^5		11.2	100	2.6×10^5
4292	$\frac{27^+}{2}$	3515	$\frac{25^+}{2}$					0.113	0.105	18.6		0.108	9.24×10^{-2}	17.4	
		3657	$\frac{25^+}{2}$					0.513	1.25	46.1	110	0.545	1.32	47.9	107
		3917	$\frac{23^+}{2}$			100		1.91	0.188	35.3		1.92	0.195	34.7	

[a] Reference 10.
[b] Calculated assuming $\epsilon_{g\,7/2}=3$ MeV.
[c] Calculated assuming $\epsilon_{g\,7/2}=4.25$ MeV.
[d] Calculated branching ratios of less than 1% are omitted.
[e] Assumed to be pure $M1$ transition (Ref. 10).

IV. SUMMARY AND DISCUSSION

An attempt has been made in this paper to explain the observed even-parity spectrum and transition rates of ^{95}Tc. The calculation followed the conventional shell-model approach. To limit the dimension of the model space a ^{90}Zr closed core has been assumed and the remaining three protons have been restricted to the $0g_{9/2}$ orbital. On the other hand, full configuration mixing has been assumed for the valence neutrons which were allowed to take all possible values in the $1d_{5/2}$, $2s_{1/2}$, $1d_{3/2}$, and $0g_{7/2}$ neutron orbitals. In order to reduce the number of adjustable parameters, the single-particle spectrum has been taken from experiment, while the effective two-body interaction has been calculated from appropriate G matrices. Thus, using only one adjustable parameter, namely the effective charge, we have reproduced, to a good approximation, the energies and transition rates of about 35 observed levels.

The present calculation differs from previous shell-model calculations[5,6] which were restricted to the $(0g_{9/2}p)^3$-$(1d_{5/2}n)^2$ basis, in the sense that a larger model space is employed for the neutrons. This expansion of the model space has been considered necessary due to the proximity in energy of the $2s_{1/2}$, $1d_{3/2}$, and $0g_{7/2}$ orbitals to the $1d_{5/2}$. This proximity suggests that a perturbation treatment of the effects of these three orbitals requires high-order corrections, a feature that is here avoided by the direct inclusion of these orbitals into the model space. This inclusion and especially that of the $0g_{7/2}$ orbital has the additional advantage that it makes the model space capable in principle of describing states that have been observed in experiment but which cannot be accommodated by the $0g_{9/2}$-$1d_{5/2}$ space. This is the case with the $\frac{29^+}{2}$ (other than the first) and with the $J^\pi > \frac{29^+}{2}$ states that have been observed in the ^{93}Nb$(\alpha, 2n\gamma)^{95}$Tc experiment[10-12] (Fig. 4). Finally, the calculated wave functions, as described in Secs. III A and III D, show that there are several low-lying states having large components outside the $0g_{9/2}$-$1d_{5/2}$ space. This feature, combined with the fact that many of these states have been identified with experimental levels, certainly makes necessary the inclusion of all the neutron orbitals into the model space.

At this point it is interesting to compare the shell-model predictions with those of the collective models. As discussed in the introduction, the most successful treatment of ^{95}Tc has been given by Bargholz and Beshai.[4] In Table IX we make a comparison of their results on the transition rates of ^{95}Tc with the predictions of the present calculation. It may be seen from Table IX that

TABLE IX. Comparison of the predictions of the collective model and the shell-model on the transitions in ^{95}Tc.

		Experiment[a]		Collective model[b]		Shell-model[c]	
		$B(M1)$	$B(E2)$	$B(M1)$	$B(E2)$	$B(M1)$	$B(E2)$
J_i	J_f	(W.u.)$\times 10^{-3}$	(W.u.)	(W.u.)$\times 10^{-3}$	(W.u.)	(W.u.)$\times 10^{-3}$	(W.u.)
$\frac{7}{2}^+$ 1	$\frac{9}{2}^+$ 1			0.17	31.6	16.9	37.3
$\frac{13}{2}^+$ 1	$\frac{9}{2}^+$ 1		35^{+24}_{-16}		24.1		29.4
$\frac{3}{2}^+$ 1	$\frac{7}{2}^+$ 1		≤ 120		13.0		32.4
$\frac{3}{2}^+$ 1	$\frac{5}{2}^+$ 1	≤ 610	≤ 300	21	38.8	0.6	85.9
$\frac{11}{2}^+$ 1	$\frac{9}{2}^+$ 1	3.3 ± 1.0	17 ± 5	19	27.0	47	9.9
$\frac{7}{2}^+$ 2	$\frac{9}{2}^+$ 1	16 ± 5	$1.9^{+1.5}_{-1.8}$	56	0.94	11	1.03
$\frac{7}{2}^+$ 2	$\frac{7}{2}^+$ 1	21 ± 7	≤ 4.5	18	18.7	51	0.048
$\frac{7}{2}^+$ 2	$\frac{5}{2}^+$ 1	94 ± 31	15^{+16}_{-22}	130	2.16	68	4.03
$\frac{11}{2}^+$ 2	$\frac{9}{2}^+$ 1	44^{+8}_{-6}	$0.43^{+0.28}_{-0.25}$	16	0.10	74.3	2.87
$\frac{11}{2}^+$ 2	$\frac{7}{2}^+$ 1		25 ± 5		21.3		18.9
$\frac{15}{2}^+$ 1	$\frac{13}{2}^+$ 1	≤ 20	≤ 29	20	16	19	2.41
$\frac{15}{2}^+$ 1	$\frac{11}{2}^+$ 1		≤ 110		28		18.5
$\frac{19}{2}^+$ 1	$\frac{17}{2}^+$ 1	38^{+26}_{-16}	$6.8^{+4.8}_{-3.8}$	8.3	10.2	59.8	2.24
$\frac{17}{2}^+$ 2	$\frac{13}{2}^+$ 1		2.4 ± 1.3		0.05		7.42
$\frac{17}{2}^+$ 2	$\frac{17}{2}^+$ 1	480^{+210}_{-110}	≤ 65	0.4	0.06	1460	0.03
$\frac{17}{2}^+$ 2	$\frac{15}{2}^+$ 1	67^{+31}_{-24}	d	2.9	16.5	135	0.126
$\frac{21}{2}^+$ 1	$\frac{17}{2}^+$ 1		$3.2^{+1.6}_{-1.3}$		53.9		17.6
$\frac{21}{2}^+$ 1	$\frac{19}{2}^+$ 1	140^{+70}_{-60}	0.7–7.1	270	1.3	170	1.18
$\frac{19}{2}^+$ 2	$\frac{17}{2}^+$ 1	0.44 ± 0.2	d	10	6×10^{-2}	0.99	2.9×10^{-4}
$\frac{19}{2}^+$ 2	$\frac{15}{2}^+$ 1		$1.7^{+0.8}_{-0.6}$		0.71		9.15
$\frac{19}{2}^+$ 2	$\frac{19}{2}^+$ 1	39^{+13}_{-10}	125^{+61}_{-44}	1.1	3.4	87.4	3.67
$\frac{19}{2}^+$ 2	$\frac{17}{2}^+$ 2	≤ 9.1	d	6.1	0.62	5.04	1.27
$\frac{19}{2}^+$ 2	$\frac{21}{2}^+$ 1	530^{+140}_{-90}	240^{+150}_{-120}	6.3	11.4	402	4.28
$\frac{25}{2}^+$ 1	$\frac{21}{2}^+$ 1		≤ 5.3		69.3		17.6

[a] Taken from Refs. 9 and 10.
[b] From the unpublished results of Bargholz and Beshai as quoted in Ref. 10.
[c] Results obtained with the Sussex interaction.
[d] Assuming pure $M1$ transition.

the two models give quite similar results with respect to $E2$ rates. Such a similarity is rewarding in view of the fundamentally different approaches that have been followed in the two calculations. On the other hand, Table IX shows that the predictions of the present calculation on $M1$ rates are generally in better agreement with experiment than those of the collective model. At this point it must be emphasized once more that the agreement of the shell-model results with experiment has been obtained without any extensive use of adjustable parameters.

Two simplifying assumptions have been made in the calculation of the effective interaction. These are (a) neglect of higher than second order terms and (b) restriction to energy denominators of $\leq 2\hbar\omega$. Moreover, in the calculation of second order terms all three-body correlations have been omitted. It requires a lengthy calculation to check whether these assumptions provide a reasonable approximation to the effective interaction, and such a calculation has not been attempted here. However, the obtained energy spectra provide an indirect justification of the approximations adopted here. For comparison two effective interactions, namely the Sussex and Yale interactions, have been used in the calculation. The results obtained from these two interactions are generally quite

similar. In the few cases where the two interactions differ, one cannot decide, due to lack of detailed experimental information, which of the two is the most appropriate.

The available experimental information on ^{95}Tc does not provide evidence that configurations other than those considered here play a vital role in the low-lying spectrum of ^{95}Tc. Such evidence can be presented by the appearance in the spectrum of ^{95}Tc of levels that cannot be accounted by our choice of the model space. As shown in Sec. III, the model predicts, up to 4 MeV, more levels than those observed in the experiment. In addition, it has been shown that the model accounts satisfactorily for the energies and transition rates of most of the observed levels.

The excitation energies of the 1085, 1179, 1747, and 2183 keV levels are not satisfactorily reproduced in the present calculation. The large energy differences are due to the fact that the identification between theoretical and experimental levels has been made by requiring agreement on transition rates rather than on excitation energies. However, it is possible that agreement with experiment on transition rates could be maintained, while the energy differences could become smaller if a different single-particle spectrum was employed. The calculations on the high-spin levels of ^{95}Tc discussed in Secs. III C and III D show that some of the properties of these levels are sensitive functions of the single-particle spectrum employed. Therefore, a more detailed calculation on ^{95}Tc ought to fit the single-particle spectrum to produce best agreement with experiment. However, such a calculation is tedious and cannot be attempted before further experimental information becomes available on ^{95}Tc. Of particular interest would be information on the spins, parities, and decay properties of the low-spin levels between 1433 and 2324 keV and on the high-spin levels above 3 MeV. Such information would also show whether some of these states belong to configurations other than those considered here.

ACKNOWLEDGMENTS

We would like to thank Dr. A. C. Xenoulis for introducing us to the problems of the Tc isotopes, and Dr. Xenoulis, Dr. T. Paradellis, and Dr. H. A. Mavromatis for many helpful discussions. Thanks are also due Mrs. K. Demakou for valuable help with the computer programs.

[1]A. Goswami and O. Nalcioglu, Phys. Lett. 26B, 353 (1968).
[2]A. Goswami, D. K. McDaniels, and O. Nalcioglu, Phys. Rev. C 7, 1263 (1973).
[3]A. C. Xenoulis, Fisika (Zagreb) 7, 97 (1975).
[4]Ch. Bargholtz and S. Beshai (unpublished), results quoted in Ref. 10.
[5]J. Vervier, Nucl. Phys. 75, 17 (1966).
[6]K. H. Bhatt and J. B. Ball, Nucl. Phys. 63, 286 (1965).
[7]M. E. Phelps and D. G. Sarantites, Nucl. Phys. A171, 44 (1971).
[8]P. D. Bond, E. C. May, and S. Jha, Nucl. Phys. A179, 389 (1972).
[9]D. G. Sarantites and A. C. Xenoulis, Phys. Rev. C 10, 2348 (1974).
[10]D. G. Sarantites, Phys. Rev. C 12, 1176 (1975).
[11]D. Hippe, B. Heits, H. W. Schuh, K. O. Zell, H. G. Freiderichs, and P. von Brentano, Z. Phys. A273, 349 (1975).
[12]T. Shibata, T. Itahashi, and T. Wakatsuki, Nucl. Phys. A237, 382 (1975).
[13]C. Dedes and J. M. Irvine, J. Phys. G: Nucl. Phys. 1, 865 (1975).
[14]C. Dedes and J. M. Irvine, J. Phys. G: Nucl. Phys. 1, 929 (1975).
[15]M. Grecescu, A. Nilsson, and L. Harms-Ringdahl, Nucl. Phys. A212, 429 (1973).
[16]J. D. Vergados and T. T. S. Kuo, Phys. Lett. 35B, 93 (1971).
[17]T. T. S. Kuo and G. E. Brown, Nucl. Phys. 85, 40 (1966).
[18]T. T. S. Kuo and G. E. Brown, Nucl. Phys. A114, 241 (1968).
[19]L. D. Skouras, H. A. Mavromatis and C. Dedes (unpublished).
[20]C. M. Shakin, Y. R. Waghmare, M. Tomaselli, and M. H. Hull, Jr., Phys. Rev. 161, 1015 (1967).
[21]J. P. Elliot, A. D. Jackson, H. A. Mavromatis, E. A. Sanderson, and B. Singh, Nucl. Phys. A121, 241 (1968).
[22]K. Krämer and B. W. Huber, Z. Phys. 267, 117 (1974).
[23]A. C. Xenoulis and D. G. Sarantites, Phys. Rev. C 7, 1193 (1973).
[24]P. Sperr, K. D. Büchs, E. Finckh, W. Fritsch, P. Pietrzyk, B. Schreiber, and A. Weidinger (private communication).